Geotextiles and Geomembranes 44 (2016) 515–533

Contents lists available at ScienceDirect

Geotextiles and Geomembranes

journal homepage: www.elsevier.com/locate/geotexmem

# Performance of geotextile filters after 18 years' service in drainage trenches

Guillaume Veylon [a, *], Guillaume Stoltz [b], Patrice Mériaux [a], Yves-Henri Faure [c], Nathalie Touze-Foltz [b]

[a] RECOVER Research Unit, Irstea, Aix-en-Provence, France
[b] HBAN Research Unit, Irstea, Antony, France
[c] LTHE Research Unit, Joseph Fourier University, Grenoble, France

ARTICLE INFO

*Article history:*
Received 6 September 2014
Received in revised form
19 January 2016
Accepted 15 February 2016
Available online 19 March 2016

*Keywords:*
Geosynthetics
Geotextile filter
Drainage trenches
Hydraulic properties
Mechanical properties
Chemical clogging

ABSTRACT

This study evaluates the long-term performance of two types of geotextiles that were used for 18 years in drainage trenches to stabilize slopes in the French Alps. The flow rate analysis of each trench enabled estimating an average permittivity at trench scale of between $10^{-5}$ and $10^{-6}$ $s^{-1}$. After exhuming the geotextiles, their hydraulic and mechanical properties were assessed. The hydraulic tests performed on geotextiles alone gave permittivities greater than $10^{-3}$ $s^{-1}$. Gradient ratio tests were performed on undisturbed soil/geotextile/drainage specimens and gave results in the order of $10^{-8}$ $s^{-1}$. The aged specimens were examined using scanning electron microscopy. Quantifying the overall performance of the geotextile filter is complicated because of the brittleness of the calcite crust and the subsequent difficulty of characterizing undisturbed interfaces. Various possible explanatory mechanisms involved in the deterioration of trench performance were reviewed: filter cake blinding, internal clogging and downstream chemical clogging. Existing analytical models were used in order to predict the loss of hydraulic performance due to each of these clogging mechanisms. By comparing the measured permittivities to the calculated permittivities, we demonstrated that chemical clogging due to calcite precipitation on the downstream face of the geotextiles was probably the preponderant mechanism responsible for the poorer performance of geotextile filters at trench scale.



## 1. Introduction

Geotextiles are used worldwide in geotechnical and geo-environmental works for filtration in drainage systems. The performance of geotextiles has been demonstrated in classical geotechnical applications by many authors (Giroud, 1982; Leflaive, 1988; Gourc and Faure, 1990; Bhatia et al., 1991; Fannin et al., 1994; Lafleur, 1999; Palmeira and Gardoni, 2000; Narejo, 2003; Palmeira et al., 2010). In particular, geotextiles are known to be an effective alternative to conventional granular filters, particularly in regions where granular materials are not available (Degoutte, 1987; Christopher and Fischer, 1992; Giroud, 1996). However, whether geotextiles can guarantee the long-term durability of installations such as hydraulic structures or drainage systems remains to be demonstrated.

The durability of geotextile filters is related to variations in the properties that allow them to perform one or more of the following functions: separation, reinforcement, filtration, drainage, protection (Koerner, 1994). Methods are now available to evaluate the durability of geotextiles in terms of the durability of their constituent fibers, which may be altered by physicochemical reactions (Cassidy et al., 1990; Mathur et al., 1994; Duvall, 1995; Hsuan et al., 2008; Van Schoors et al., 2009). However, even if the geotextile fibers themselves are undamaged, the performance of geotextile filters may be reduced in terms of filtration and flow capacities.

The main mechanism affecting the durability of geotextile filters used in drainage systems is clogging, which occurs on the scale of the entire geotextile filter. A geotextile filter is composed not only of the geotextile itself but also includes the interface between the geotextile and the natural soil (filter cake or bridge) and between the geotextile and the drainage material (downstream crust). A

* Corresponding author. RECOVER Research Unit, Irstea, 3275 Route Cézanne, CS 40061, 13182 Aix-en-Provence cedex 5, France. Tel.: +33 490424936; fax: +33 442668865.
*E-mail address:* guillaume.veylon@irstea.fr (G. Veylon).

http://dx.doi.org/10.1016/j.geotexmem.2016.02.002
0266-1144/

geotextile filter should thus be considered as a filtering zone that evolves over time (see Fig. 1), and its clogging can be caused by physical, biological, and/or chemical processes (Koerner et al., 1988; Rollin and Lombard, 1988).

The mechanism behind physical clogging is the accumulation of fine particles within the geotextile or upstream of the geotextile filter (Giroud, 1996; Palmeira and Gardoni, 2000). Internal physical clogging results from the accumulation of material within the voids between the geotextile fibers. The subsequent decrease in effective porosity and in the interconnectedness of the pore network reduces the hydraulic conductivity of the geotextile, which may reduce filtering and draining efficiency. External physical clogging, or "blinding" as described by Faure and Fry (2004), is caused by the formation of a granular filter cake (or filter bridge) upstream of the geotextile, which may progressively clog the geotextile by retaining increasingly finer particles (Christopher and Fischer, 1992). Intensive research on this phenomenon led to the development of models (Faure et al., 2006) and standardized tests (Luettich et al., 1992; Mlynarek, 1998). The design guidelines are generally based on empirical approaches and are expressed in terms of retention and permeability criteria (Christopher and Fischer, 1992; Heerten, 1993; Lafleur et al., 1992; Giroud, 1996; Lafleur, 1999). Applying these methods requires assessing the properties of the filtrated soil or bedding material (Giroud et al., 1990; Wu et al., 2006; Palmeira et al., 2012) and examining in situ conditions such as confining stress (Palmeira and Gardoni, 2002). However, although the physical clogging of geotextiles can significantly degrade the hydraulic performance of drainage systems, their drainage and filtration properties generally remain acceptable. For example, Faure et al. (1999) filter geotextiles used for 21 years in the Valcros embankment dam (France) were exhumed and studied. The authors main conclusion was that the geotextile properties had not been significantly altered. The most severe degradation in mechanical performance had occurred when installing the geotextile and biochemical effects were negligible. Despite particle impregnation ranging from 15% to 30%, the geotextile still performed its filtration and drainage functions.

Biological clogging requires very specific physicochemical conditions in terms of temperature, alkalinity (Halse et al., 1987), and concentrations of minerals and organic substances (Fleming and Rowe, 2004). Extensive analysis of the mechanisms involved has led to the identification of the relevant parameters and to models of the physicochemical processes (Cooke et al., 1999; Cooke and Rowe, 2008; Yu and Rowe, 2012). Geotextile clogging seems to occur with the following stages: formation of surface biofilms, generation of slimes, and the growth and interconnection of bioconcretions. These structures can be stabilized by the precipitation of low-solubility sulfide and carbonate minerals, and the subsequent decrease in the geotextiles porosity is accelerated by the entrapment of fine particles from the soil being drained (Rowe, 2005; Rowe and Yu, 2010). For geotextiles used in leachate-collection systems, field studies (Koerner and Koerner, 1995; Junqueira et al., 2006; Fleming et al., 2010) and laboratory experiments (Koerner and Koerner, 1992; Mendonca and Ehrlich, 2006; Palmeira et al., 2008) demonstrated the importance of biological clogging in the degradation of drainage systems, showing that this type of clogging is a major concern for drainage in leachate-collection systems. However, in conventional drainage systems, organic acids in water are generally present only at low concentrations, so biological clogging is not expected to be a significant factor.

Very few full-scale experiments or field studies have found chemical clogging of geotextile filters to be a determining phenomenon. McIsaac and Rowe (2006) simulated full-scale collection systems permeated with real municipal solid-waste leachate. They allowed these systems to evolve for six years and studied how different filter designs influenced the clogging process and the extent of clogging under full-scale and real-time conditions. Based on laboratory measurements and microscopic-scale analyses, they showed that the clogging of nonwoven needle-punched geotextiles was primarily due to the development of chemical clogs within the fibrous structure of the geotextile and that the loss of hydraulic conductivity (more than 90%) did not cause leachate ponding. Testemale et al. (1999) studied the geotextile installed between the original embankment and the downstream reinforcement berm at

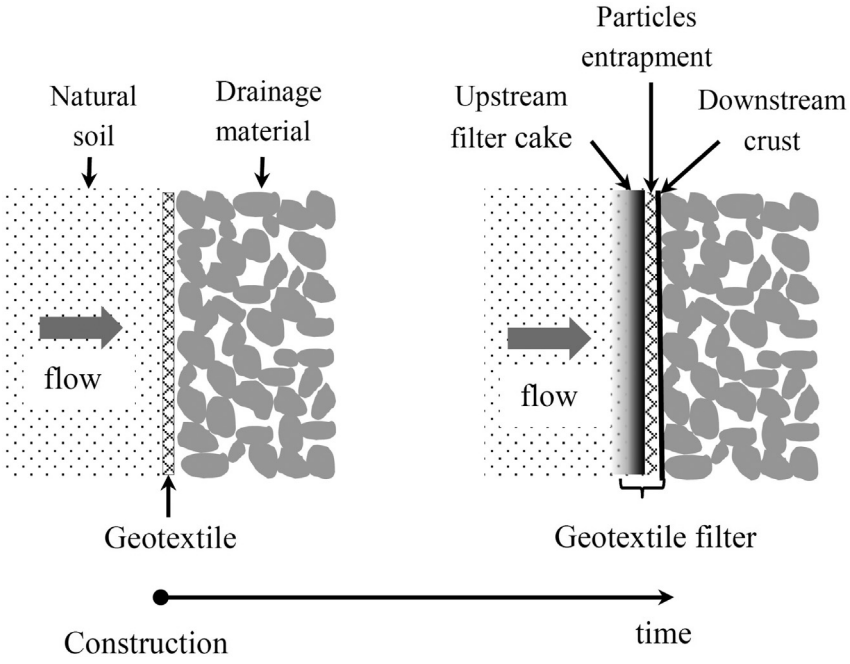


**Fig. 1.** Evolution of the geotextile filter structure over time.

the Torcy-Vieux embankment dam. The combination of unfavorable conditions (i.e. the presence of dispersive clay, percolation of an iron oxide solution, and significant organic content in the drained water) resulted in the geotextile being clogged by the precipitation of iron oxide onto the geotextile fibers and the subsequent trapping of eroded clay particles.

In the present work, to investigate the different clogging mechanisms influencing the long-term behavior of geotextile filters used in drainage trenches, a campaign to dismantle 18-year-old drainage trenches was performed. During exhumation, the geotextile filters, including the geotextiles and their interfaces with the natural soils and drainage materials, underwent careful and detailed visual inspection. Two trenches equipped with two different types of geotextiles were investigated. The exhumed geotextiles were subjected to mechanical and hydraulic experiments. Any variation over time of the geotextiles properties was determined by comparing the mechanical and hydraulic properties of aged products measured in the laboratory with the results of the same measurements made on virgin products. The results were interpreted using observations of the phenomena at the microscopic scale. The goal of this report is to quantify the long-term evolution of the mechanical and hydraulic properties of geotextile filters and to identify the primary physicochemical mechanisms that cause them to become clogged.

## 2. Materials and methods

### 2.1. Experimental site

The Trièves region (Isère, France), located approximately from 20 to 50 km south of Grenoble (Fig. 2), is the region of the French Alps with the highest exposure to landslides. The main factor explaining this predisposition to instability is the presence of massive deposits of glaciolacustrine clays, called *Trièves clays*, dating from the Quaternary period (Würm). Trièves clays have a silty clay texture. Between 20 and 45% of the particles have a diameter less than 2 μm (Fig. 3) which gives them poor mechanical and physicochemical properties. Their low plasticity index ($9 \leq PI \leq 25$) and liquid limit ($29 \leq LL \leq 50$) makes them likely to move quickly from a plastic to a liquid state due to natural fluctuations in water content (van Genuchten and van Asch, 1988; van Genuchten, 1989; Giraud et al., 1991).

The Trièves clays are finely laminated with light colored silty beds alternating with dark colored clayey beds. The thickness of these laminae is variable (1–100 mm) and their orientation is quasi-horizontal. The textural anisotropy conjugated with cracks parallel to the bedding planes also affects the hydraulic properties of the clays. The permeability is of the order of $10^{-10}$ m/s perpendicular to the bedding planes whereas it reaches $10^{-9}$ to $10^{-8}$ m/s parallel to the bedding planes (Nieuwenhuis and Van Genuchten, 1986).

Given the very low permeability of soils and the localized character of flow paths, the most effective way to achieve stabilization is with drainage trenches. In these specific hydrogeological conditions where the goal is to intercept localized flow paths, high-speed flows favor soil erosion, so fine-particle suspensions may contribute to clogging the geotextile filter. The stabilization operation consisted of constructing four drainage trenches (T2 to T5) by excavating the trenches and then filling them with a high-permeability drainage material (30–50 mm calibrated rolled and washed gravel) (Veylon et al., 2012). Trench T2 served as the control trench and was only equipped with a horizontally oriented geotextile covered with a topsoil layer. Trenches T3 to T5 were equipped with geotextiles arranged over the entire periphery of the drainage trench (Fig. 4). Each trench was 12 m long and between

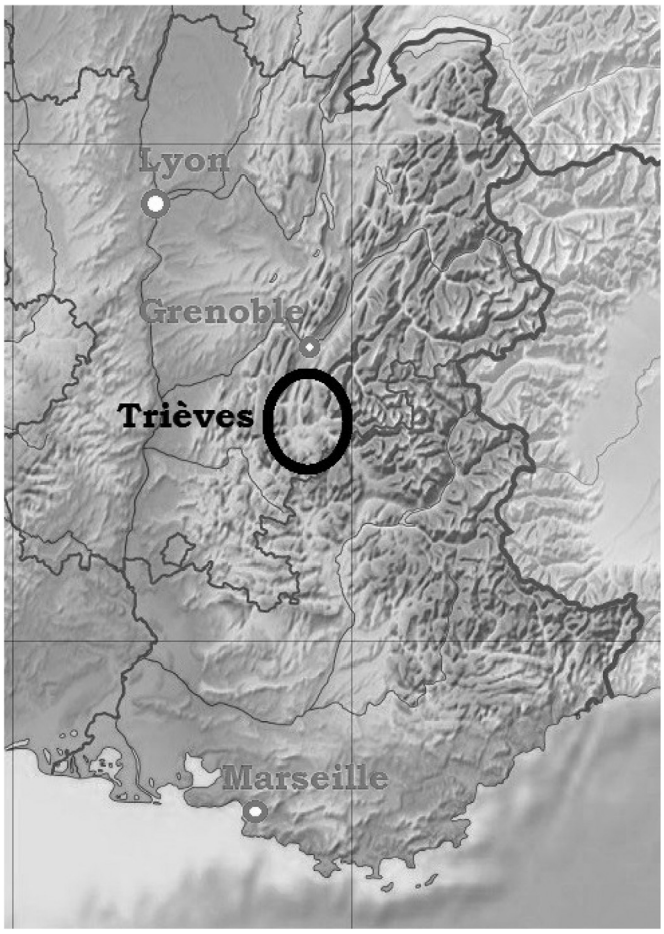


**Fig. 2.** Location map of the Trièves region.

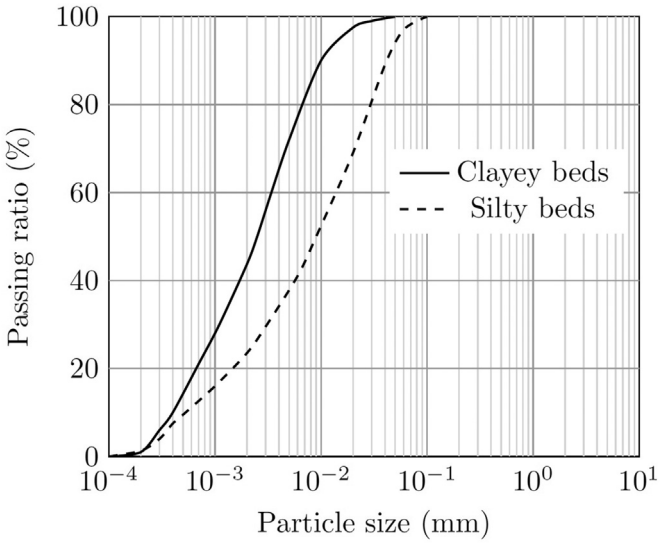


**Fig. 3.** Grain-size distribution of the different beds composing the varved clays.

1.50 and 2.50 m deep. Their performance was monitored by periodically measuring the drained flows and upstream groundwater levels. The present study focuses only on the control trench without geotextiles (trench T2) and the trenches equipped with nonwoven needle-punched geotextiles (trench T3) and woven-strip

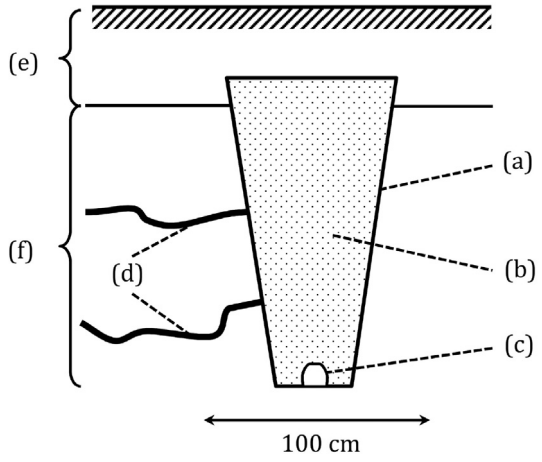


**Fig. 4.** Schematic view of the cross section of trenches T3 and T4: (a) geotextile filter, (b) drainage material, (c) drain and (d) flow channels from the varved clays. The stratigraphy of the soil adjacent to the trenches is composed of (e) a topsoil layer and (f) the varved clay layer.

geotextiles (trench T4) with filter pores of comparable size (see Table 4). Trench T5 was not included in the study because the hydraulic conditions proved to be very different from the other trenches.

### 2.2. Flow rate measurements

The measurements of the drainage flow rates of the trenches were monitored during two distinct phases: from 1993 to 1999 and from 2008 to 2011. No measurements were made between 1999 and 2008. During the periods monitored, the measurements were made manually with calibrated buckets approximately every 20 days.

### 2.3. Specimen collection program

The dismantling work consisted of carefully dismantling six meter long segments of each trench. The upstream soil and the gravelly drainage material were excavated from the top to the bottom in vertical steps of 0.5 m (Fig. 5).

For each trench, the sampling protocol for laboratory measurements was as follows:

- obtain a remoulded sample of drainage material at the bottom of the trenches to determine the fine content,
- obtain a sample of the drain at the bottom of the trench to estimate the apparent clogging rates of the slots,
- obtain a geotextile specimen (about 5 $m^2$) to determine permittivity, opening size, and tensile strength,
- obtain three specimens of varved clays for identification (grain size distribution, Atterberg limits, etc.),
- obtain two specimens of downstream calcite crust for chemical analyses,
- obtain three specimens of interface soil/geotextile/pebbles for gradient-ratio (GR) measurements on undisturbed specimens.

Geotextile aging was examined by comparing the mechanical and hydraulic characteristics of virgin specimens with those of aged specimens. Depending on the trench under consideration, the initial characteristics of the geotextiles were determined by following one of the two strategies outlined below. All geotextile specimens were acquired following the standard NF EN ISO 9862 (AFNOR, 2005). For trench T3, only a single 200 mm × 300 mm virgin geotextile specimen was available. This specimen had been stored for 18 years in a cabinet, during which time it had not been exposed to direct light. However, this virgin specimen was too small for conducting new measurements according to current standards, so the data for this specimen were taken from the product datasheet delivered by the manufacturer when the geotextile was installed. Thus these data were obtained according to the standards applicable in 1993 (AFNOR, 1989; AFNOR, 1983), which differed significantly from the current standards (AFNOR, 2010b, 2010a), especially for the opening size test in terms of testing protocol and representative passing ratio (Table 3). For trench T4, a large virgin geotextile specimen was also stored for 18 years in a cabinet away from direct light. This specimen was sufficiently large to measure its properties according to current standards. Thus, for trench T4, both the virgin geotextile and the exhumed geotextile were measured according to current standards.

### 2.4. Tensile tests

The maximum tensile strength (a mechanical property) was also determined. The small size of the virgin T3-geotextile specimen required that the tensile measurement was performed according to standard NF EN ISO 13934-1 (AFNOR, 1999) instead of standard NF EN ISO 10319 (AFNOR, 2008).

### 2.5. Fine content within the drainage material

The fine content within the drainage material was estimated according to the French standards (AFNOR, 1996). The test consists in separating the agglomerated grains by mixing the drainage material under water. Then the particle-size distribution of the soil, once dried, was established by sieving it through successively smaller meshes and weighing the cumulated fractions that did not pass through them.

### 2.6. Filtration opening size measurements

The filtration opening size measurements were performed according to European standards (AFNOR, 2010b). The test was performed by cutting five samples of geotextiles, placing the samples securely in metal sieves, and adding a known quantity of calibrated sand of known particle size distribution on top of the material. The sand was sprayed with water and the sieves were mechanically shaken at a frequency between 50 and 60 Hz for ten minutes to induce particle movement through the geotextile. The particle size distribution of the particles that passed through the geotextile was determined. The filtration opening size $O_f$ was defined by the $d_{90}$ of the material that passed through the geotextile. It indicated the approximate largest particle that could pass through the geotextile.

### 2.7. Hydraulic tests

Standard hydraulic tests were performed on nonwoven needle-punched (trench T3) and woven strip (trench T4) geotextiles. In the permittivity tests from the former standards (AFNOR, 1983), flow rates were imposed and the corresponding hydraulic heads measured. The tests were performed for different flow rate values and the permittivity was estimated as the slope of the linear curve representing the flow rate as a function of the water head. In the permeability tests (AFNOR, 2010a), the permeability normal to the plane was estimated for an imposed value of hydraulic head loss equal to 50 mm and the corresponding flow rate was measured.

The hydraulic tests performed on the aged products were conducted with great care. Indeed, various compounds (calcite, clay

**Fig. 5.** Dismantling work of a trench.

particles, etc.) were embedded in the pores of the exhumed geotextiles. These compounds formed a kind of inhomogeneously distributed crust on the geotextile. Inside the trenches, and in particular inside trench T3, the geotextiles were in contact with gravel, and the geotextile surface was clean at these contact points, (i.e. there was no crust). These clean areas of the geotextile could be preferential paths through which the opening size and hydraulic conductivity could be measured (permeability normal to the geotextile plane). To evaluate the effect of these paths, similar measurements were performed on clean areas of geotextiles that were impregnated with paraffin wax (Palmeira and Matheus, 2000). These additional measurements gave similar results, indicating that the preferential paths had no effect. Therefore only the results from specimens without paraffin wax are presented.

Moreover, permeability measurements are index measurements that call for procedures that may not be appropriate for certain aged products. Indeed, as per the standard NF EN ISO 12956 (AFNOR, 2010b), the permeability measurement required several operations that may modify the properties of the geotextiles. In particular, before performing the measurement, the prewetting operation requires saturating the product for at least 12 h with a wetting agent. Since this operation may dissolve certain calcite compounds, several supplementary measurements were performed without this prewetting step. Based on these measurements, the prewetting step was observed to have no significant effect. The permeability measurement also required a hydraulic head of at least 50 mm capable of leaching the embedded compounds. Because the standard requires the water flow to be measured three times for each specimen, special care was taken to avoid increasing the water flow during the measurement. During short measurements (about 10 min), there was no change in the water flow, indicating that the results for permeability normal to the geotextile plane were not affected by the leaching of embedded particles or calcite dissolution.

The hydro-mechanical effect of water flow on calcite crust may have an influence on the hydraulic behavior of the geotextile. Thus the hydraulic permeability measurements were also performed following an adapted column test procedure. To avoid leaching of the crust due to hydromechanical action, geotextiles samples were sandwiched between two layers of standard sands. The presence of sand intended to ensure the maintenance of the crust of calcite during the test. A layer of sand of thickness 50 mm was placed at the base of an oedometric cell 100 mm in diameter. The 120 mm diameter geotextile sample was placed gently on the sand. The cell body was then assembled with the base and a layer sand 30 mm thick was then deposited on top of the geotextile. After slow saturation of the sample from below, an upward flow at very low gradient was applied across the sample with water tanks at constant level upstream and downstream. A differential pressure sensor connected upstream and downstream of the cell, measured the difference in total pressure of the flow directly. The hydraulic head loss due to the geotextile was evaluated from the hydraulic head loss measurements and flow speeds, using Equation (1):

$$\Delta h = \Delta h_t - \frac{Q}{S}\frac{d_s}{k_s} \tag{1}$$

where $\Delta h$ is the hydraulic head loss due to the geotextile, $\Delta h_t$ is the total hydraulic head loss through the whole specimen, $k_s$ the permeability of the sand ($=5\cdot10^{-3}$ m/s) and $d_s$ is the total thickness of the sand layers.

The hydraulic performance was estimated at different scales (trench, interface, geotextile) and under various hydraulic heads. Thus the pertinent property for comparing the results of the

different hydraulic measurements is the permittivity, which can be evaluated as follows:

$$\psi = \frac{Q}{S\,\Delta h} \tag{2}$$

where $S$ is the section of the drainage surface ($m^2$), $Q$ the flow rate passing through the filter ($m^3/s$) and $\Delta h$ is the hydraulic head loss (m). Under operational conditions, the flow rate and water head loss are generally proportional (Ling and Tatsuoka, 1993), i.e. the regime of the water flow passing through the filter can be considered as laminar (van der Sluys and Dierickx, 1987).

### 2.8. Gradient ratio measurements

Gradient-ratio measurements (GR) were performed on intact specimens including the interfaces between the soil and the geotextile and between the geotextile and the drainage material. Initially, the specimens taken from the site were destined for GR measurements in oedometer cells with vertical flow or in rectangular tanks (300 300 700 $mm^3$) with horizontal flow. The GR measurements performed in these cells with rigid walls were abandoned for the following reasons: the rigid walls facilitated the preferential flow along these walls, and saturating the specimens by applying back pressure was very difficult due to the material at hand. Therefore these measurements were performed in triaxial cells large enough to accommodate 150-mm-diameter specimens.

The samples were cut with great care to avoid remoulding the interface. Each sample was coated with bentonite in order to prevent lateral bypassing of the water flows. Before the positioning of the membrane, a hole was made in the varved clays in order to set the pressure sensor about 25 mm upstream the geotextile. Finally, the upper part of the sample containing the pebbles was filled with 5–10 mm diameter gravels to ensure the mechanical stability of the specimen 6. The test protocol was based on the ASTM 5101 Standard (ASTM, 1996): a vertical upward flow of water was directed through a specimen comprising (in the flow direction) 100 mm of the soil to be measured, a geotextile, and drain gravel. The pressure loss of the flow was measured through the soil along a path of length $l_s$ (around 75 mm) and through the filtering zone comprising the geotextile and a length $l_f$ of soil in contact with the geotextile (around 25 mm) (Fig. 6). The behavior of the soil/geotextile/pebbles interface, which was assumed to also be that of the geotextile filter, is characterized by the ratio:

$$GR = \frac{i_f}{i_s} = \frac{h_f / l_f}{h_s / l_s} \tag{3}$$

where $i_s$ is the reference hydraulic gradient in the soil measured in a region away from the geotextile, and $i_f$ is the hydraulic gradient across the filter. This measurement was performed after three days of saturation under low confining stress (50 kPa). When GR = 1, the filter has the same permeability as the ground. If GR < 1, the filter becomes more permeable than the soil. GR > 1 indicates clogging in the filter.

The advantage of this measurement is that it is not necessary to measure the flow for clayey soils. However, the challenge of this measurement is to detect a significant pressure within the soil at 25 mm from the geotextile. The main difficulty with the GR measurement is to prepare a 150-mm-diameter cylindrical specimen without moving the gravel or breaking the bridges linking the calcite crust and the pebbles, which possibly calls for cutting the largest pebbles with a circular saw, cutting the geotextile without lifting off the soil, and cutting the varved clay specimen without fracturing the specimen. A pore-waterpressure sensor was connected to a piezometer and a volume controller used to determine the volume of water injected into the specimen. Monitoring water levels in the upstream and downstream cruets verified mass balance for the flow. The advantage of this apparatus is, firstly, it prevents preferential flow paths (the membrane is pressed against the flexible walls of the specimen) and, secondly, it applies back pressure to help saturate the specimen.

### 2.9. Microscopic views

Stereomicroscopy (SM) was used to visualize the upstream and downstream faces of the exhumed geotextiles at the millimeter scale. Scanning electron microscopy (SEM) was used to investigate geotextile clogging and blinding at the fiber and particle scale. The specimens used for these analyses were taken from a calcified zone of the downstream interface.

### 2.10. Chemical analyses of water

The temperature and pH of the water drained from the outlet of the trenches were measured. The pH was measured using a pH meter and a calibrated glass electrode. The values measured were then corrected to account for the water temperature. Chemical analyses

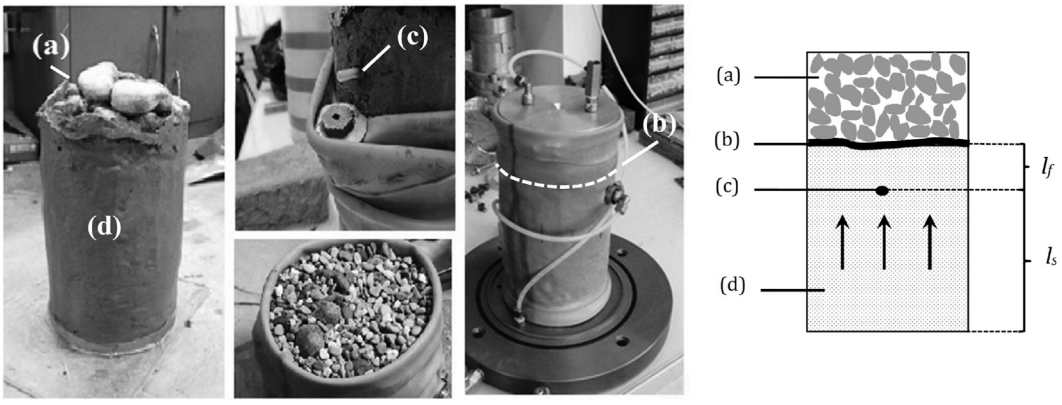


**Fig. 6.** Preparation of the samples for gradient ratio measurements: (a) downstream drainage material, (b) geotextile layer, (c) measurement point of the upstream pore-water pressure and (d) upstream drained soil coated with bentonite.

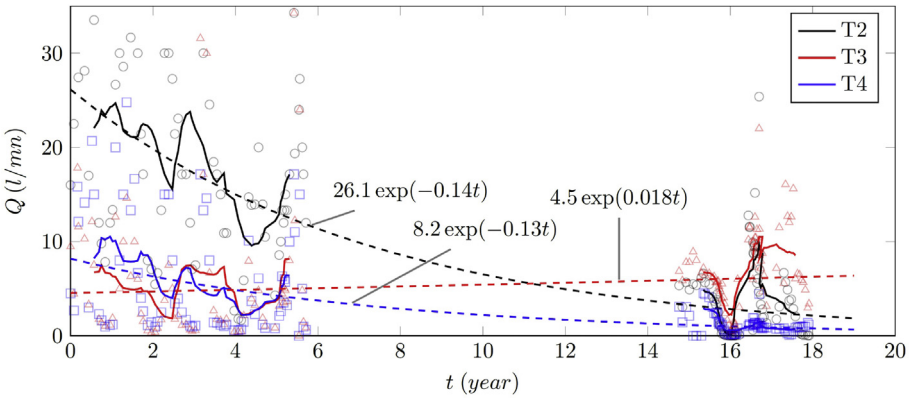


**Fig. 7.** Evolution of flow rate measurements for the control trench (T2), the trench equipped with a nonwoven needle-punched geotextile (T3) and the trench equipped with a woven strip geotextile (T4). The measures are represented by dots and the solid curves represent the moving average curves for a time widow equal to one year. The dashed curves are exponential regression curves.

were performed to determine the mineral concentration in the water of chloride, sulfate, bicarbonate, calcium, magnesium, and sodium.

### 2.11. Chemical identification of soil and crust material

The chemical compositions of the varved clays, upstream cakes, and downstream crusts of trenches T3 and T4 were determined by Inductively Coupled Plasma-Atomic Emission Spectrometry (Murray et al., 2000) after alkaline fusion (Dean, 1974; Germanique, 1994; Sounga et al., 2012). The carbonated fraction was analyzed as per the protocol and classification proposed by Miche et al. (2013).

### 2.12. X-ray diffraction

X-ray diffraction (XRD) was used to determine the mineralogy of the varved clays (the clayey and silty beds were analyzed separately), filter cakes, and encrusted material acquired downstream of each geotextile. All XRD data were collected under the same experimental conditions and in the angular range $0° < 2\theta < 35°$. Prior to XRD measurements, all the specimens were decarbonated in hydrochloric acid and rinsed. The organic content was removed with disodium peroxodisulphate. The remaining sediment was suspended using an ultrasound bath and left to decant for two hours. The fraction of sediment finer than 2 μm was subsequently removed and concentrated into a clay paste with a centrifuge. For each specimen, this clay concentrate was used to prepare three slides: an untreated control slide (U), a heated slide (H), and a glycolated slide (G). The slides were analyzed with a Philips PW1050-81 diffractometer equipped with a cobalt anode. The mineralogy of the clay in each specimen was based on changes in the spectral signature after physical and chemical treatments. The clay content was semiquantified with the spectral signatures and peak areas from the glycolated slides. The intensities of the various peaks were subsequently weighted and transformed into percentages (Moore and Reynolds, 1989).

## 3. Results

### 3.1. Hydraulic performance of the trenches

The flow rate measurements showed great dispersion, suggesting that the hydrogeological behavior of the site was quite complex. Moving average curves were plotted to highlight the long-term trend of the flow rate evolutions. The time window of the moving average was chosen equal to one year to limit the effect of seasonal fluctuations due to hydrological and physico-chemical phenomena.

The analysis of moving average curves (Fig. 7) shows that over the 18 years of the experiment, trenches T2 (control) and T4 (woven-strip geotextile) suffered significant decreases in hydraulic performance. During the same period, the flows drained by trench T3 (nonwoven needle-punched geotextile) increased slightly.

Let us denote $Q$ the mean flow rate drained by the trench over one year. It is possible to define the clogging rate, corresponding to the relative decrease of the flow rate due to clogging between $t$ and $t + \Delta t$ as the ratio $\Delta Q/Q$. It is reasonable to assume that it is constant, i.e. that the seasonal fluctuations do not influence the long-term trend. Thus it is possible to perform an exponential regression on the moving average curves of trenches T2 and T4. The evolution of the mean annual flow rate $Q$ can be expressed according to Equation (4):

$$Q = Q_0\, e^{-\lambda t} \tag{4}$$

where $Q_0$ is the value of the mean annual flow rate at the beginning of the experiment and $\lambda$ is the annual clogging rate representing the mean value of the ratio $\Delta Q/Q$. The results of the regression analysis are shown in Table 1. The values of $Q_0$ show that the mean flow rate initially drained by trench T2 is three times the flow rate drained by trench T4. The clogging rates for both trenches T2 and T4 have very close values between 0.13 and 0.14. From the practical standpoint, this means that the trench drainage capacity of trenches T2 and T4 decreases by almost 15% per year. These results tend to demonstrate that the geotextile of trench T4 has little effect on the clogging mechanism occurring in the trenches. Trench T3 has a negative clogging rate, suggesting that some of the flow rates originally drained by the neighboring trenches T2 and T4 may have been

**Table 1**
Regression parameters determined from the analyses of the flow rates of each trench and parameters used to determine the field permittivity over the period 2008–2011.

| Trench | T2 | T3 | T4 |
|---|---|---|---|
| *Regression analysis* | | | |
| $Q_0$ (l/mn) | 26.1 | 4.5 | 8.2 |
| $\lambda$ | 0.14 | −0.018 | 0.13 |
| $R^2$ | 0.59 | 0.67 | 0.79 |
| *Field permittivity* | | | |
| $Q_f$ (l/mn) | 0.5–16.1 | 2.4–11.3 | 0.5–1.6 |
| $H_w$ (m) | 1.3 | 1.0 | 1.0 |
| $\psi_f$ ($s^{-1}$) | $0.1–2.0\cdot10^{-5}$ | $0.7–3.1\cdot10^{-5}$ | $1.4–4.4\cdot10^{-6}$ |

diverted to the trench T3 or that a moderate internal erosion mechanism within the varved clays may have been initiated.

An average field permittivity for each trench was also estimated from the field measurements using Equation (2). The drainage surface was approximately equal to the product of $H_w$, the height of the water table upstream of the trench (measured by the mean of the piezometers), by $L$, the total length of the trench ($\approx$12 m). Assuming a linear increase of the hydraulic head with depth, the average hydraulic head $\Delta h$ was then approximated to $H_w/2$. Here, the representative flow rate $Q_f$ is the instantaneous value restricted to the case where the water table remains contained within the varved clays. The field data are given in Table 1.

### 3.2. Field observations

Details of the observations made during exhumation are available in Veylon et al. (2012). The following main conclusions were drawn from the field observations (Table 2):

- Preferential flow paths within the varved clays took the form of pipes with diameters up to 20 mm perpendicular to the trench axis,
- A granular filter cake was formed on the upstream side of the geotextiles. A network of channels developed within the granular filter cake, tangent to the geotextile plane. This network appears to have still been functioning in trench T3 (Fig. 8(a)) but had been filled with fine roots in trench T4 (Fig. 8(b)),
- A crust formed on the downstream side of the geotextile for trenches T3 and T4. This crust was also present on the soil/gravel interface in control trench T2 (Fig. 9(a)). In all the trenches, the gravelly drainage material was locally embedded in the crust (Fig. 9(a)–(c)).

The drains were inspected using a camera supported by a frame equipped with wheels (Fig. 10). The amount of sediment deposited on the bottom drain varied from one trench to another. The thickness of sediment reached 20 mm in the drain of trench T2. Roots with diameters up to several millimeters had developed within the sediment layer. For trench T4, fine roots (less than one millimeter in diameter) were observed in the sediment layer whose thickness was of the order of 5–6 mm. For trench T3, the sediment thickness did not exceed 4–5 mm and was free of roots.

**Table 2**
Initial characteristics of the geotextiles and observational data on the geotextiles, the drains and the drainage material.

| Trench | T2 | T3 | T4 |
|---|---|---|---|
| *Virgin geotextile characteristics* | | | |
| Polymer | / | Polyethylene | Polypropylene |
| Fabric | / | Nonwoven | Woven strip |
| $\mu_g$ (kg m$^{-2}$) | / | 0.13 | 0.19 |
| $t_g$ (mm) | / | 1.3 | 0.7 |
| *Field observations* | | | |
| $t_f$ (mm) | 30–40 | 10–20 | 20–30 |
| $t_c$ (mm) | 1–2 | 0–1 | 1–2 |
| $t_d$ (mm) | 18–20 | 4–5 | 5–6 |
| *CR* | 73% | 21% | 16% |
| *FC* | 12% | 1% | 2% |

$m_g$: mass per unit area of the geotextile
$t_g$:thickness of the geotextile
$t_f$: thickness of the upstream cake.
$t_c$:thickness of the downstream crust.
$t_d$: thickness of the sediment inside the drain.
*CR*: apparent clogging rate of the drain.
*FC*: fine content (<50 μm) within the drainage material.

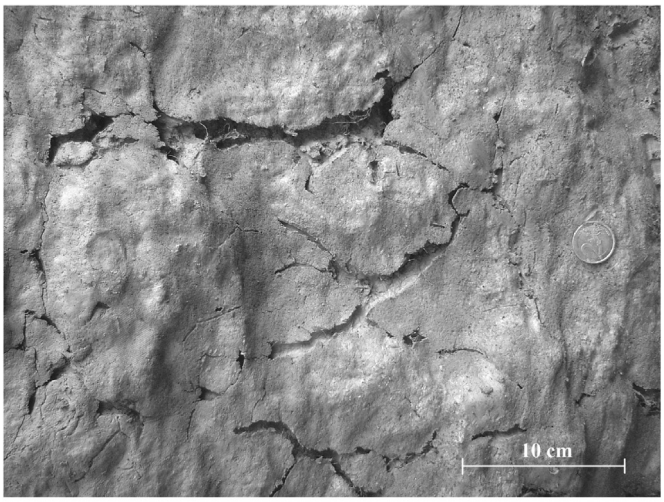


(a)

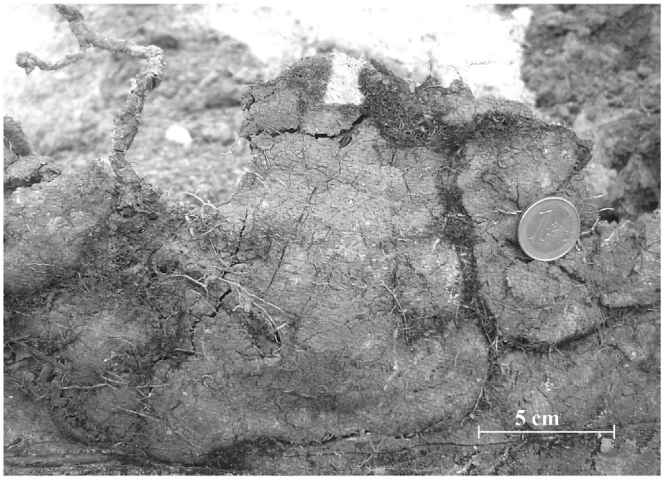


(b)

**Fig. 8.** Flow channels through the granular cake upstream of the geotextiles. (a) Trench T3 (nonwoven needle-punched geotextile), (b) Trench T4 (woven strip geotextile).

The slotted drains at the bottom of the trenches were partially clogged with clay and/or calcite concretions. The apparent clogging rates varied from 16 to 21% for the trenches equipped with geotextiles. In the control trench, however, the apparent clogging rate reached 73% (Table 2).

### 3.3. Fine content within the drainage material

The fine content within the drainage materials was measured between 1 and 2% for the trenches equipped with geotextiles and reached 12% for the control trench without geotextile (Table 2).

### 3.4. Opening size measurements

The photographs of the specimens clearly show the imprint of pebbles in the downstream crust for both nonwoven needle-punched and woven-strip geotextiles (Fig. 11). The opening size of the exhumed geotextiles (Table 3) was 25%–30% lower than that of the virgin products. The opening size of the geotextile from trench T3 decreased slightly in comparison to that of the virgin product, but this result questionable because the opening size for

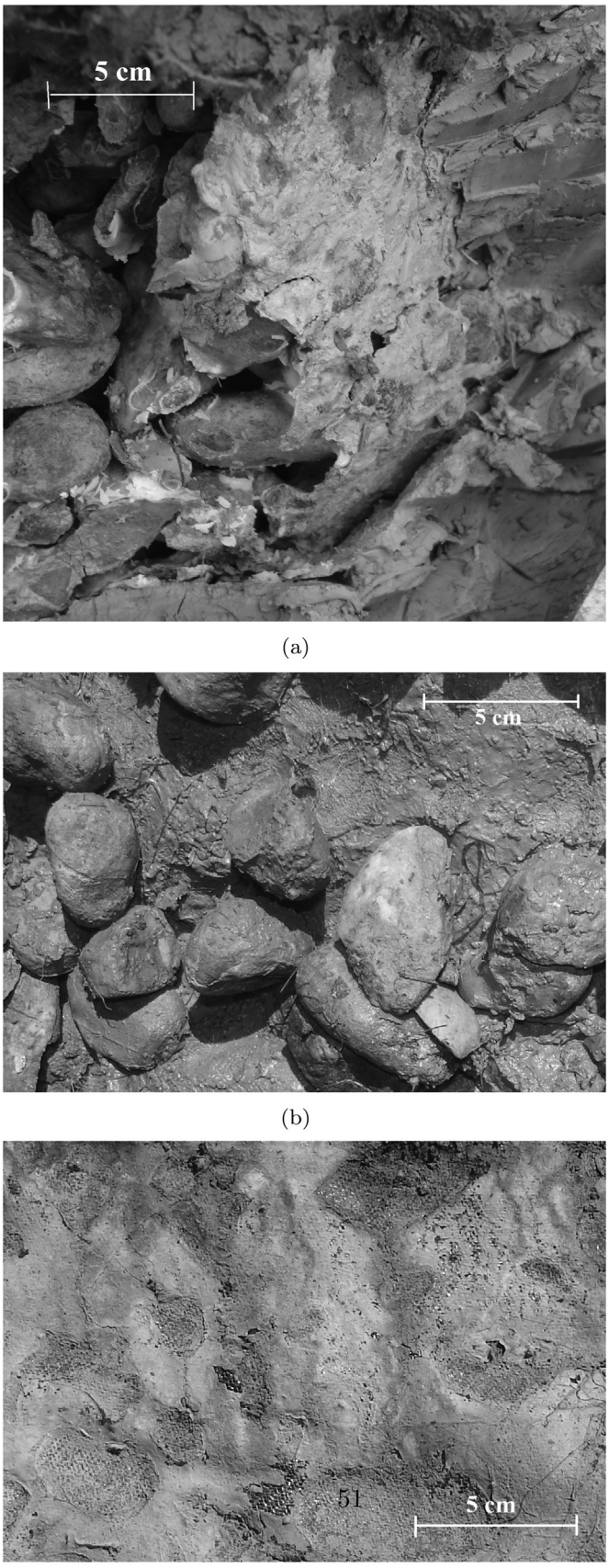


**Fig. 9.** Calcified interface between the drainage material (pebbles) and the downstream calcite crust for (a) control trench T2, (b) trench T3 (nonwoven needle-punched geotextile), and (c) trench T4 (woven strip geotextile).

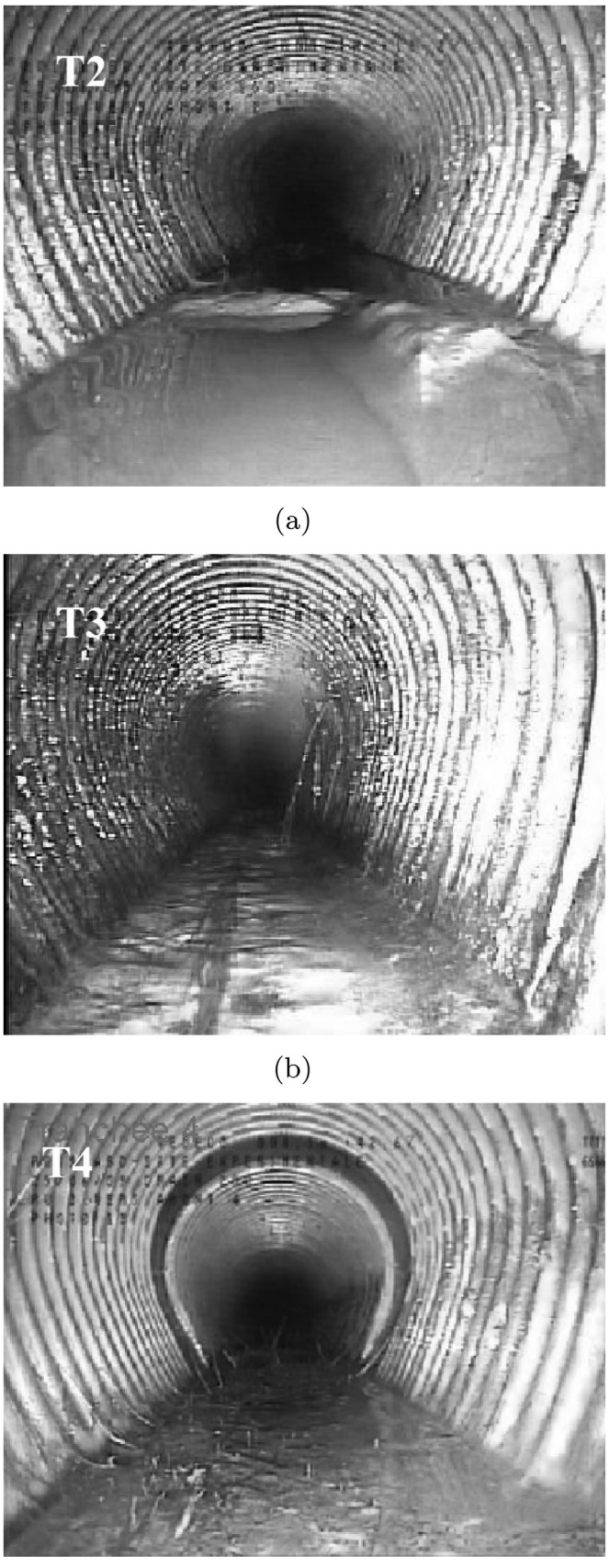


**Fig. 10.** Visual inspection of the bottom drains (a) trench T2, (b) trench T3 and (c) trench T4.

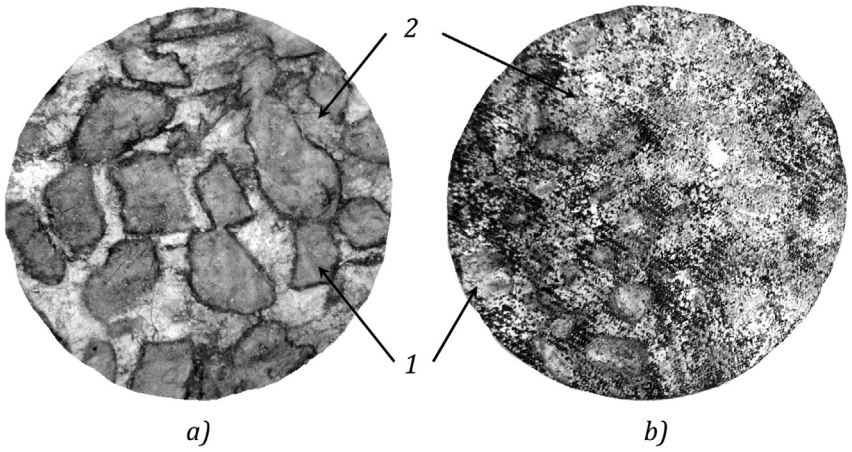


**Fig. 11.** Downstream side of the typical geotextile specimen used for opening size measurements exhumed from trenches (a) T3 and (b) T4. 1: pebble prints, 2: calcite deposits.

**Table 3**
Laboratory tests performed on the geotextiles. Each test was conducted on 5 specimens per geotextile.

| | trench T3 | | trench T4 | |
|---|---|---|---|---|
| | Virgin | Exhumed | Virgin | Exhumed |
| Mass per unit area | | | | |
| $\mu_g$ (kg m$^{-2}$) | 0.13 | 0.76–1.09 | / | / |
| Filtration opening size $d_{90}$ (μm) | | | | |
| Opening size tests (AFNOR, 2010b) | 140[a] | 96 ± 17 | 163 ± 24 | 123 ± 24 |
| Hydraulic permittivity $\psi$ (s$^{-1}$) | | | | |
| Permittivity tests (AFNOR, 1983) | 4.6[b] | 0.78 ± 0.73 | n/a | n/a |
| Permeability tests (AFNOR, 2010a) | n/a | 0.58 ± 0.53 | 0.26 ± 0.06 | $6.8 \pm 2.2 \cdot 10^{-2}$ |
| Column tests | n/a | $6.1 \pm 2.8 \cdot 10^{-2}$ | n/a | $5.2 \pm 2.1 \cdot 10^{-4}$ |
| Tensile tests (AFNOR, 1999) | | | | |
| Tensile strength (N) | 264 ± 76 | 298 ± 74 | 2042 ± 40 | 1909 ± 107 |
| Strain at burst (%) | 50.5 ± 4.8 | 36.7 ± 3.6 | 17.1 ± 0.9 | 15.7 ± 1.2 |

n/a: not applicable.
[a] Manufacturer's data $d_{95}$ (μm) from AFNOR (1989).
[b] Manufacturer's data from AFNOR (1983).

the virgin product was taken from the datasheet and was therefore determined with the earlier standard NF G 38016 (AFNOR, 1983).

### 3.5. Permittivity measurements

Based on the results of the standardized hydraulic tests (Table 3), the permittivity values decreased by a factor of five for geotextile T3and by a factor of four for the geotextile T4. The higher dispersion in the results of the exhumed products (Table 3) may be understood by examining the photographs of the specimens (Fig. 12) which show that the material embedded in the geotextile pores is heterogeneous.

The permittivity measurements performed on the exhumed products in the column tests resulted in the demonstration of lower values of permittivity by one order of magnitude for the nonwoven needle-punched geotextile (T3) and by two orders of magnitude for the woven strip geotextile (T4). The significant difference observed for the woven strip geotextile may be explained by the fragility of the calcite compounds embedded in the interstices between the stripes (Figs. 17(b) and 18(b)) that were probably removed and leached away at the beginning of the application of the hydraulic head of 50 mm. The leaching mechanism is less pronounced if the geotextile is maintained by soil on its interfaces. This may explain why the permittivity values obtained from column tests are much lower than in permeability tests.

### 3.6. Tensile tests

The tensile measurements of the exhumed geotextiles (Table 3) showed no significant change in the mechanical characteristics with respect to the virgin products. However, the strain at burst of the exhumed T3 geotextile decreased significantly, indicating that the fibers stiffened. This effect could be explained by the physico-chemical evolution of the constituent polyethylene fibers over time.

### 3.7. Gradient ratio measurements

Fig. 13 shows an example (trench T3) of the progression of the volume of water injected during the GR measurement and the pore-water pressure upstream of the filter. The results presented in Table 4 show that all trenches were concerned by clogging. Moreover, the results suggest that clogging of the filter containing the nonwoven needle-punched geotextile in trench T3 ($1.9 \leq GR \leq 5.7$) was slightly more pronounced than in the filter containing the woven-strip geotextile in trench T4 ($1.0 \leq GR \leq 1.5$). However, the bond between the fibers of the nonwoven needle-punched geotextile and the calcite crust likely led to less remolding of the interface. For the woven-strip geotextile, calcified particles were less encrusted in the geotextile and the crust peeled and cracked more easily. Thus the results may not accurately reflect the in situ

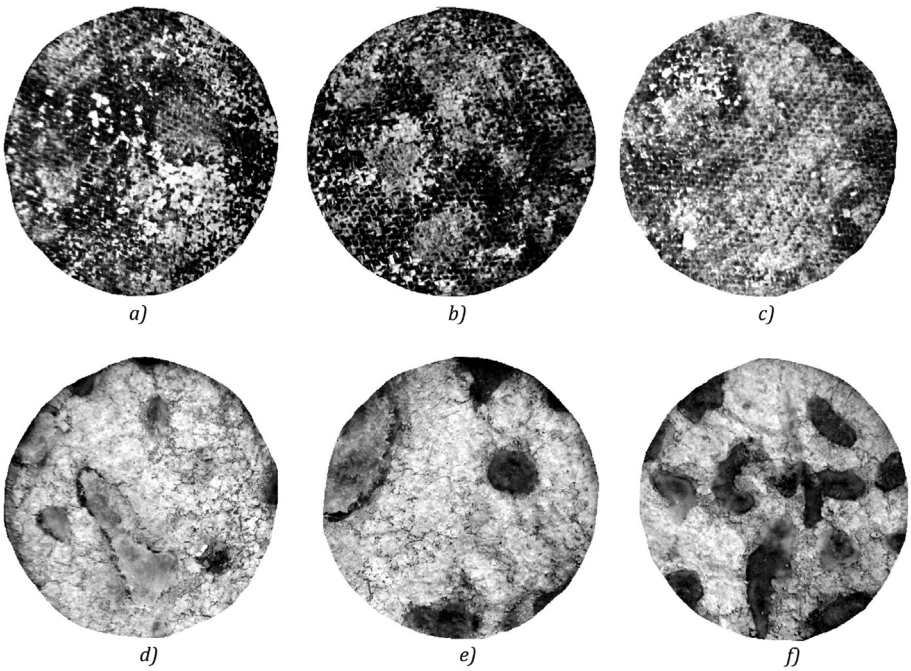


**Fig. 12.** Examples of geotextile specimens exhumed from trenches T3 [(d) (f)] and T4 [(a) (c)]. The permeability characteristics of these specimens were obtained normal to the plane of the geotextile.

properties of the filtering interface due to the practical difficulties of this measurement.

### 3.8. Microscopic views

SEM images of the upstream face of the nonwoven needle-punched geotextile (T3) show that some fibers were wrapped locally in a cluster of fine particles (Fig. 14) measuring between 0.1 and 0.5 mm in diameter. The micron-scale views show a large amount of clogged material within the geotextile. Locally, the geotextile appears completely clogged (Fig. 15(b)), but a significant amount of voids still remains (Fig. 15(a) at the scale of several square millimeters).

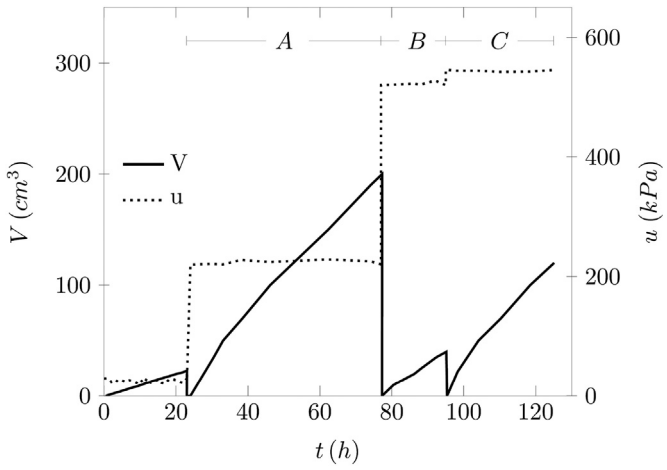


**Fig. 13.** Typical results of gradient ratio measurements on undisturbed specimens (nonwoven needle-punched geotextile from trench T3, here). The solid line labeled *V* indicates the injected volume of water; the dashed line labeled *u* indicates the pore-water pressure upstream of the filter. Labels A, B and C refer to the loading phases corresponding to the three confining pressures and counter pressures.

The downstream face of the geotextile showed a quasi-continuous crust (Fig. 16). The micron-scale observations of nonwoven needle-punched geotextile reveal a porous assembly of calcite crystals (grain size ≈10–30 μm) which contain macropores and channels. The apparent surface density of these channels ranges from 0.3 to 0.4 per square millimeter. The channels seem to widen in the direction of water flow from upstream to downstream. From the visual standpoint, the control section of the channel ranges from 30 to 90 μm, with a mean value around 50 μm which corresponds to three times the dimensions of the particles. It is noteworthy that these extreme values correspond to three times the dimensions of the particles and that the upper value has the same order of magnitude as the filtration opening sizes of the geotextiles.

The woven-strip geotextile did not appear to be significantly damaged (Figs. 17(b) and 18(b)). A dense crust composed of fine particles appeared upstream of the geotextile. This crust is particularly developed at the intersection between the strips (Fig. 17(b)). The crust contains visible cracks, suggesting that it may have been degraded during sampling. As a preliminary remark, it is important to note that the SEM images of the downstream face of the geotextile were acquired from specimens from which a large portion of the calcite crust deposited on its surface was removed during dismantling. However, the pollution of the geotextile on the downstream side is similar to that on the upstream side but spans a wider area (Fig. 18(b)). When the crust was not removed during the dismantling work, the downstream face of the geotextile also showed a quasi-continuous crust (Fig. 18(a)). The micron-scale observations downstream of the woven strip geotextile also revealed a porous microstructure containing macropores and channels. The apparent surface density of these channels was lower than that of the nonwoven needle-punched geotextile (from 0.1 to 0.2 per square millimeter). The stereomicroscope views show that the dimensions and geometry of the channels did not present significant differences from those of the nonwoven needle-punched geotextile (Fig. 18(a)).

**Table 4**
Parameters and results of the gradient ratio measurements performed in the triaxial cell.

| Specimen | $l_s$ (mm) | $l_f$ (mm) | $\sigma_3$ (kPa) | $u_{cp}$ (kPa) | $i$ | $\psi$ ($s^{-1}$) | $h_s$ (m) | $h_f$ (m) | $GR$ |
|---|---|---|---|---|---|---|---|---|---|
| T2-1 | 72 | 25 | 70 | 0 | 40 | $1.9 \cdot 10^{-8}$ | 2.42 | 1.58 | 2.0 |
| | | | 500 | 400 | 40 | $1.6 \cdot 10^{-8}$ | 2.57 | 1.33 | 1.5 |
| | | | 500 | 400 | 60 | $2.3 \cdot 10^{-8}$ | 4.00 | 2.00 | 1.5 |
| T3-1 | 80 | 25 | 300 | 200 | 19 | $10.8 \cdot 10^{-8}$ | 0.78 | 1.22 | 5.0 |
| | | | 600 | 500 | 19 | $7.2 \cdot 10^{-8}$ | 1.51 | 0.49 | 1.0 |
| | | | 600 | 500 | 38 | $6.0 \cdot 10^{-8}$ | 2.52 | 1.48 | 1.9 |
| T3-2 | 75 | 25 | 500 | 400 | 40 | $4.8 \cdot 10^{-8}$ | 1.94 | 2.06 | 3.2 |
| | | | 500 | 400 | 80 | $4.8 \cdot 10^{-8}$ | 2.75 | 5.25 | 5.7 |
| T4-1 | 178 | 22 | 500 | 400 | 22 | $3.6 \cdot 10^{-8}$ | 4.21 | 0.79 | 1.5 |
| T4-2 | 75 | 25 | 400 | 300 | 40 | $13.2 \cdot 10^{-8}$ | 2.98 | 2.98 | 1.0 |
| | | | 500 | 400 | 40 | $10.8 \cdot 10^{-8}$ | 2.66 | 2.66 | 1.5 |

$l_s$ = length of the flow path through the soil; $l_f$ = length of the flow path through the filter; $\sigma_3$ = confinement pressure; $u_{cp}$ = counter pressure; $i$ = total applied gradient; $\psi$ = permittivity of the geotextile filter; $h_s$ = Differential water head through the soil; $h_f$ = Differential water head through the filter; $GR$ = gradient ratio.

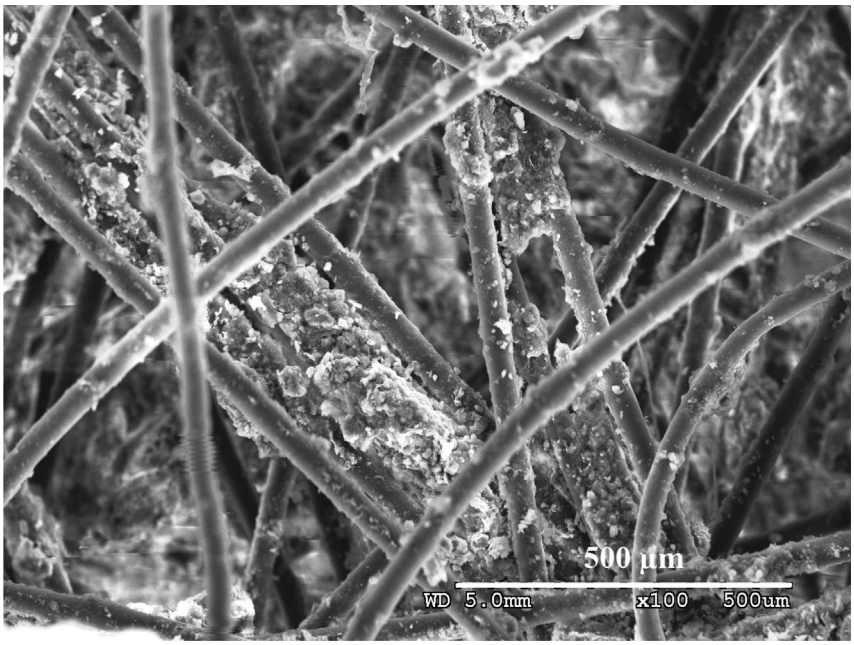


**Fig. 14.** Micron-scale view of the internal clogging mechanism developing around the fibers of the nonwoven needle-punched geotextile (trench T3).

### 3.9. Chemical composition of water

The temperature of the water drained by the trenches varied between 6°C (early March) and 14 °C (early September), and its *pH* varied spatially and temporally between 7.0 and 8.2. Chemical analyses revealed that the calcium carbonate saturation index ranged from 0.6 to 0.9 (Table 5). The water was supersaturated with $CaCO_3$ and precipitation was expected.

### 3.10. Chemical composition of soil and crust material

Based on the chemical analyses (Table 6), most of the carbon in the material encrusted on the geotextiles was in the form of inorganic compounds, assumed to be calcite. The other material embedded in the geotextile pores may be clay particles from the upstream natural soil.

### 3.11. X-ray diffraction

The phases were identified by comparing the XRD peak positions and intensities against reference data (Moore and Reynolds, 1989). The diffractograms of the clay fraction for the clayey beds were similar to those for the silty beds. The XRD results for the clay fraction of the upstream cake and downstream crust are also similar, so only one of these diffractogram is shown (Fig. 19). The results for the three specimens obtained from three different preparation methods show that the predominant phases of the specimens were illite (d ≈ 10.05 to 10.08 Å), chlorite (d ≈ 14.03 to 14.30 Å), and expansive clays (d ≈ 10.52 to 13.13 Å). The expansive clays were interstratified illite/smectite rich in illite (Table 6).

## 4. Discussion

The results of the mechanical measurements confirmed the conclusions regarding the aging of geotextiles based on visual and microscopic-scale observations. The mechanical characteristics of the geotextiles had remained the same since their installation in 1993. These results were consistent with the apparent integrity of the geotextile fibers observed in the SEM images.

The observational results showed that the presence of geotextile had a beneficial impact on the apparent clogging rates of the slotted drains, on the fine content within the gravelly drainage material and on the amount of material found in the bottom drains.

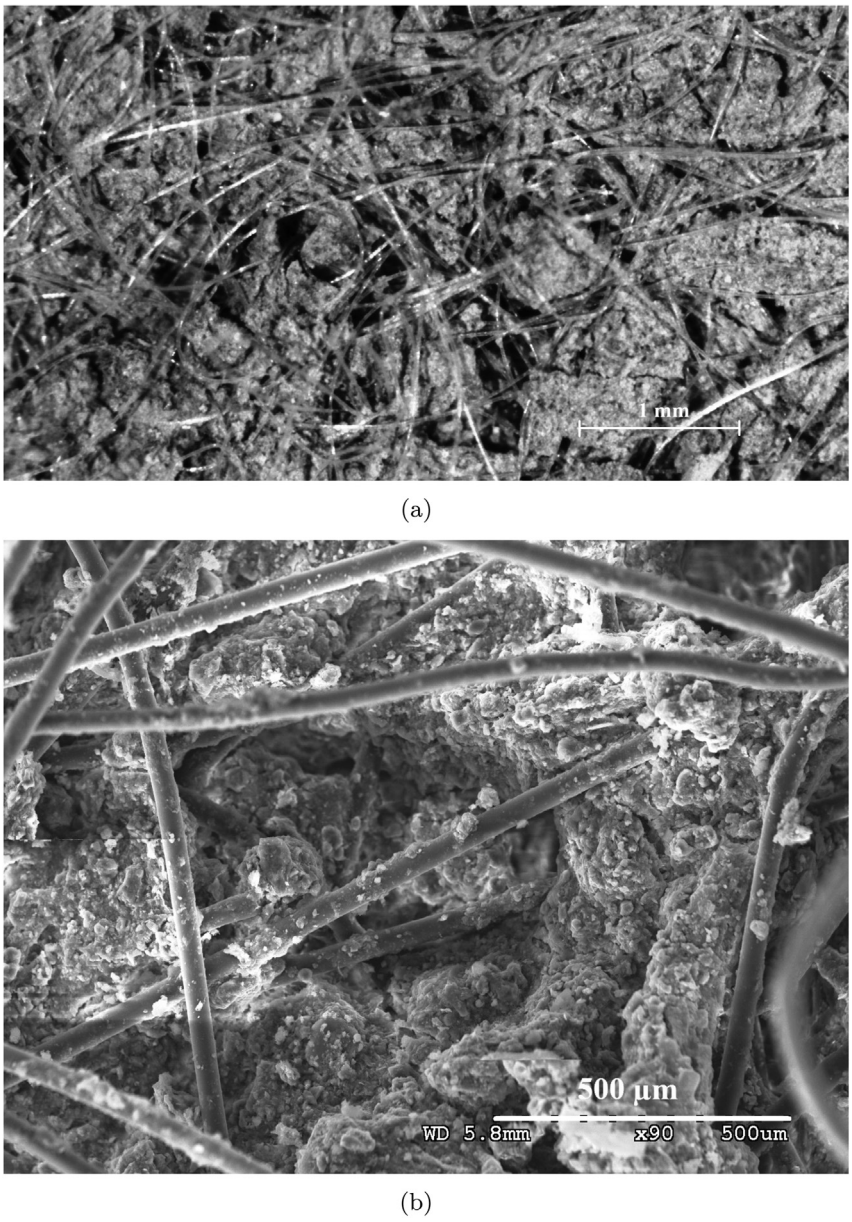


**Fig. 15.** Micron-scale views of the upstream side of the nonwoven needle-punched geotextile (trench T3) with (a) stereomicroscope and (b) SEM.

Moreover, the low clogging rate of the drains at the bottom of the trenches and the low fine contents within the drainage material for the trenches equipped with geotextiles suggested that the loss of hydraulic performance can be attributed to the soil/geotextile/pebbles interfaces.

The results described in the present study showed that the geotextile filters were subjected to three phenomena that potentially altered their filtration performance: *i)* blinding due to the formation of a granular filter cake upstream of the geotextiles, *ii)* internal clogging of the geotextiles by fine particles, and *iii)* the formation of a porous calcite crust on the downstream face of the geotextile.

### 4.1. Blinding

Our observations indicate the presence of granular filter cakes upstream of the geotextiles. These agree with many observations made in situ and in the laboratory (Kossendey, 1999).

For trench T3, equipped with a nonwoven needle-punched geotextile, the presence of a network of flow channels tangent to the geotextile plane indicated the capacity of the flow to bypass blinded areas of the geotextile. Thus the filter cake blinding the geotextile was not sufficient to clog the entire geotextile filter. Flow channels also developed in trench T4, equipped with a woven-strip geotextile. However, these channels were filled with roots, and the small diameter of these roots supports the idea that these channels were colonized by plant roots after the geotextile was completely clogged.

The presence of these channels may also explain why the permittivity values of the whole geotextile filter (GR tests) were much smaller than the values deduced from the tests on geotextiles only. On the GR tests, the flow canals were absent or not connected to the flow source due to the size of the samples. Thus the water was forced to flow through the upstream filter cake. The chemical analyses on the upstream filter cake showed that it was composed

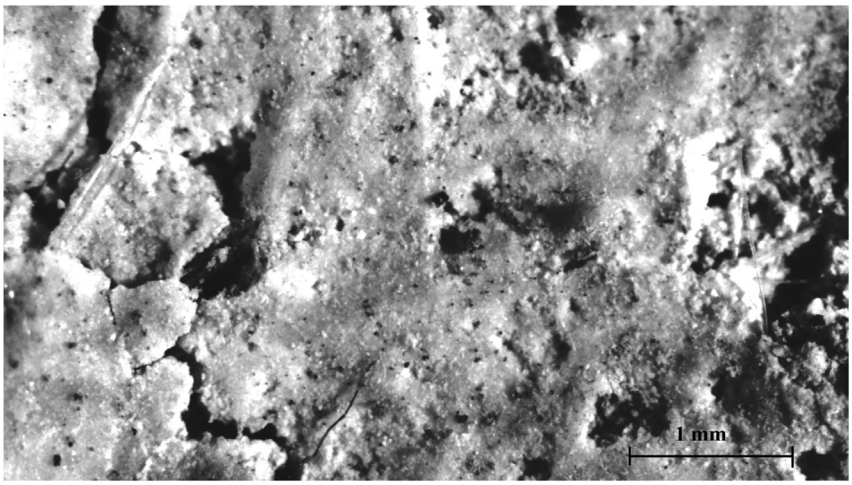


(a)

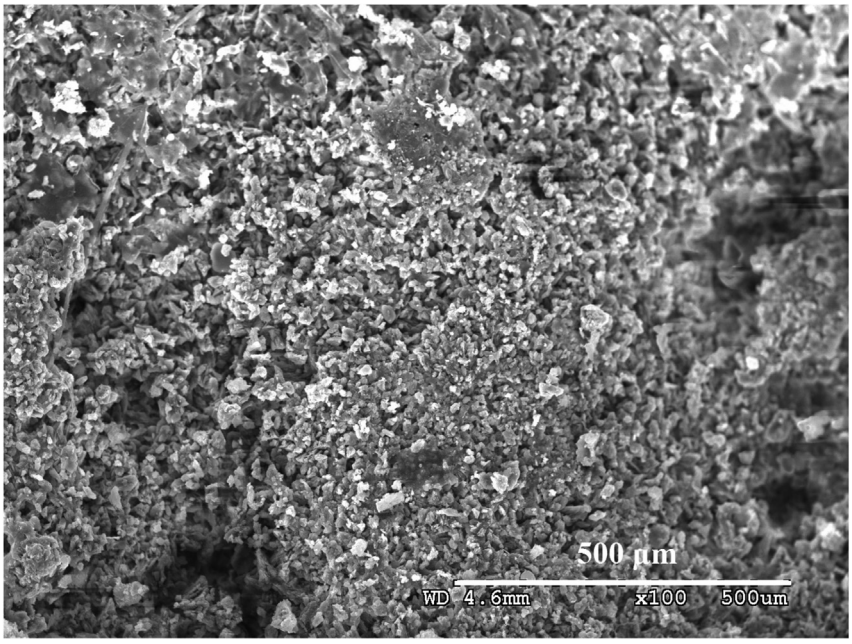


(b)

**Fig. 16.** Micron-scale views of the upstream side of the nonwoven needle-punched geotextile (trench T3) with (a) stereomicroscope and (b) SEM.

of varved clays (T4) with a small proportion of organic matter from which dissolved CaO, MgO and MnO components were removed.

The permeability of the filter cake can be roughly estimated from the empirical relationship with the void ratio ($e$) and the limidity index ($LI$) (Carrier and Beckman, 1984) given by Equation (5):

$$k = \frac{1}{1+e}\left(\frac{LI+0.242}{95.21}\right)^{4.29} \quad (5)$$

Applying Equation (5) using the identification characteristics of the varved clays ($LI = 0.3 - 0.5$), the measured thicknesses of filter cakes (Table 2) and by postulating $e = 0.8 - 1.0$, we obtained a range of permeability values from $1.3 \cdot 10^{-10}$ to $5.7 \cdot 10^{-10}$ m/s, which is in accordance with the hydraulic conductivity values also proposed by other authors (Luettich et al., 1992). This range of values corresponds to an interval of permittivities between 1.0 and $50.0 \cdot 10^{-8}$ $s^{-1}$ for trench T3 and between 0.5 and $25.0 \cdot 10^{-8}$ $s^{-1}$ (Fig. 20). These values are comparable to the permittivity values obtained from the GR tests performed on the whole geotextile filter.

Our analysis demonstrates that the results of the *GR* tests are representative of the hydraulic behavior of the upstream filter cake. Moreover, it suggests that the blinding of the geotextile by the filter cake was not the mechanism responsible for the deterioration of the hydraulic performance of the trenches.

### 4.2. Internal clogging

The filtration opening sizes of the geotextiles evolved over the 18 years of service. The opening sizes of trenches T3 and T4 decreased by 30% and 25% respectively. According to the particle size distribution of the varved clays, the filtration opening sizes were larger than the maximum particle dimension of the varved clays. The filter rules were far from being fulfilled and most of the upstream material should not have been retained on or within the geotextiles. However, the MEB images of the T3 geotextile clearly

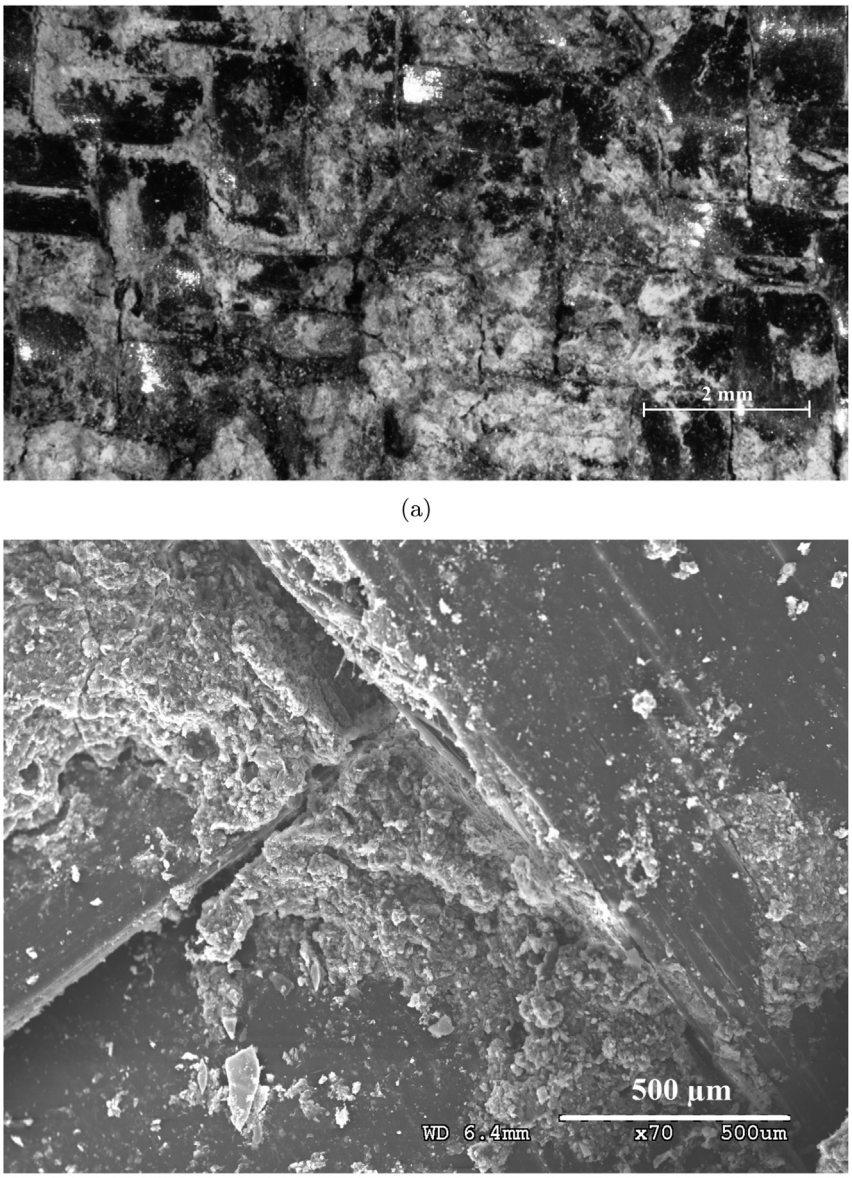


**Fig. 17.** Micron-scale views of the upstream side of the woven strip geotextile (trench T4) with (a) stereomicroscope and (b) SEM.

demonstrate that internal clogging occurred and suggest that the hydraulic properties of the geotextiles could be significantly impacted. The development of the downstream calcite crust was probably responsible for the retention of the particles inside the geotextile.

The micron-scale views show that agglomerates developed at the surface and around the fibers (Fig. 14). Thus, in order to evaluate the effect of internal clogging on geotextile performance, the permittivity was evaluated using the formulation developed by Palmeira et al. (2008) for the case of bacteria films attached to the fiber surfaces. Their expression of the permeability coefficient k can be written according to Equation (6):

$$k = \frac{\beta \rho_w g}{16 \eta_w} \frac{\left(d_f / 4\right)^2}{1-n} \frac{(n - n\mu/\mu_{max})^3}{1 - n + n\mu/\mu_{max}} \tag{6}$$

where $\beta$ is a shape factor, taken as equal to 0.11 according to Giroud (1996), $\rho_w$ is the water density (1000 kg/m$^3$), $g$ is the acceleration of gravity (9.81 m/s$^2$), $\eta_w$ is the dynamic viscosity of the water ($10^{-3}$ Pa.s), $d_f$ is the diameter of the fibers (35 µm), $n$ is the geotextile porosity (0.93), $\mu$ is the mass of clogging material within the geotextile per unit area whose maximum value is given by:

$$\mu_{max} = n\rho' t(1 - n') \tag{7}$$

where $\rho'$ is the density of the agglomerate (2000 kg/m$^3$), $t$ is the thickness of the geotextile and $n'$ is the porosity of the agglomerate (0.5). The mass measurements performed on the aged geotextiles gave $\mu = 0.83$–$0.96$ kg/m$^2$ (Table 2). Based on visual observations on aged products, we assumed that the thickness of the geotextile remained unchanged $t = 1.3$ mm. The permeability coefficient of the aged product accounting for internal clogging was of the order

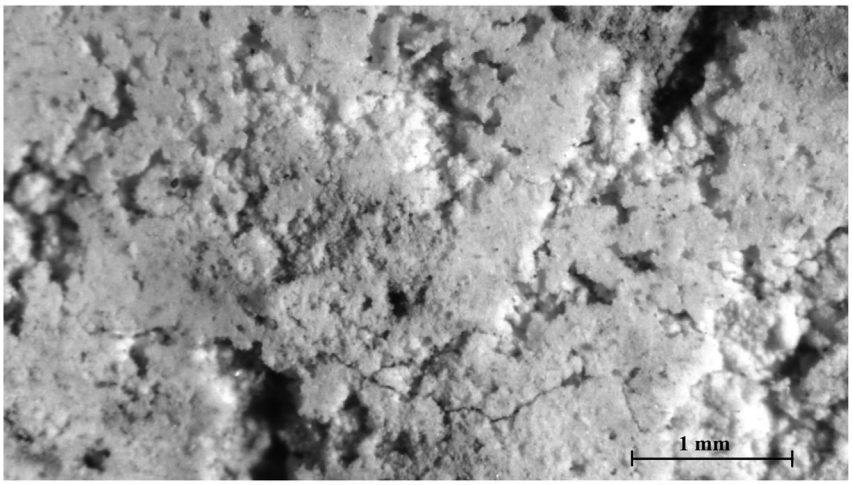


(a)

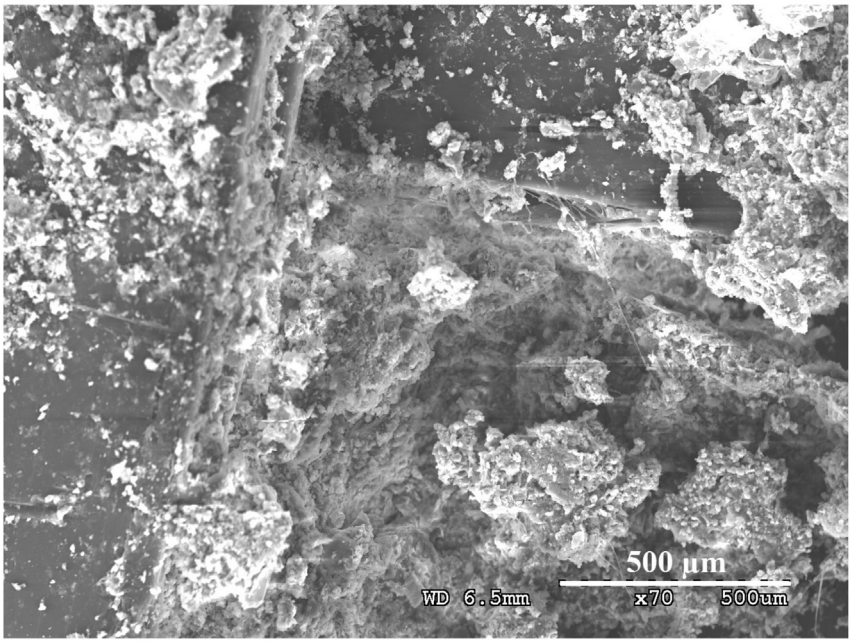


(b)

**Fig. 18.** Micron-scale views of the upstream side of the woven strip geotextile (trench T4) with (a) stereomicroscope and (b) SEM.

**Table 5**
Results of the chemical analyses performed on the water.

| Trench | T2 | T3 | T4 |
|---|---|---|---|
| *Physical characteristics* | | | |
| T (°C) | 9 | 12 | 10 |
| pH | 7.5 | 7.9 | 7.8 |
| *Concentrations (mmol/l)* | | | |
| $Mg^{2+}$ | 0.69 | 0.92 | 0.98 |
| $Ca^{2+}$ | 14.2 | 12.7 | 13.5 |
| $HCO_3^-$ | 5.9 | 5.0 | 5.4 |
| *Calcium carbonate saturation index* | | | |
| SI | 0.6 | 0.9 | 0.9 |

of $2.5–6.6 \cdot 10^{-6}$ m/s for clogging ratios $\mu/\mu_{max}$ ranging between 59% and 69%.

These conclusions are consistent with other long-term-performance analyses (Mannsbart and Christopher, 1997; Faure et al., 1999). These results indicate that, even for highly polluted geotextiles, the degradation of the hydraulic characteristics can remain limited. This conclusion is also consistent with the work of Palmeira and Matheus (2000), who artificially clogged nonwoven needle-punched geotextiles with paraffin to simulate different levels of clogging. Using GR measurements performed on various clogged geotextiles, they observed that a decrease of geotextile porosity from 90% to 42% did not induce a significant increase in GR. Only a strong decrease of geotextile porosity (lowered to 34%) allowed them to detect geotextile impregnation by the paraffin with GR measurements.

The range of permittivity values obtained from the analytical model for the nonwoven needle-punched geotextile (T3) is $1.9–9.1 \cdot 10^{-3}$ $s^{-1}$. These values are two orders of magnitude lower than the permittivity values deduced from the permittivity tests and one order of magnitude lower than the permittivity values deduced from the column tests performed on the geotextiles alone (Fig. 20). Thus, these tests may not be representative of the effect of

**Table 6**
Chemical composition, mineralogy of carbonate and clay fractions of the varved clays, the upstream filter cake and the downstream crust of the geotextiles expressed in % weight.

| Trench | Varved clays | | T3 | | T4 | |
|---|---|---|---|---|---|---|
| | Cb | Sb | Uc | Dc | Uc | Dc |
| *Chemical analyses* | | | | | | |
| MO | 4.71 | 5.99 | 8.16 | 2.18 | 4.35 | 1.11 |
| $SiO_2$ | 42.27 | 44.60 | 60.48 | 4.75 | 44.96 | 2.10 |
| $Al_2O_3$ | 15.85 | 15.59 | 13.63 | 2.15 | 14.09 | 1.26 |
| $Fe_2O_3$ | 4.85 | 4.95 | 5.15 | 0.41 | 4.77 | 0.15 |
| CaO | 15.31 | 15.13 | 6.12 | 50.72 | 15.37 | 54.10 |
| MgO | 1.72 | 1.58 | 0.96 | 0.29 | 1.53 | 0.22 |
| $K_2O$ | 2.78 | 2.76 | 2.33 | 0.27 | 2.50 | 0.13 |
| MnO | 0.26 | 0.18 | 0.08 | 0.01 | 0.22 | 0.02 |
| $Na_2O$ | 0.70 | 0.75 | 0.62 | 0.08 | 0.93 | 0.01 |
| LOI-MO | 11.58 | 9.78 | 4.83 | 37.83 | 11.63 | 40.42 |
| *Mineralogy of carbonate* | | | | | | |
| Calcite | 24 | 23 | 9 | 90 | 24 | 96 |
| Dolomite | 5 | 4 | 2 | 1 | 4 | 1 |
| Residue | 71 | 73 | 89 | 9 | 72 | 3 |
| *Mineralogy of clay fraction* | | | | | | |
| Chlorite | 7 | 6 | 3 | 5 | 5 | 3 |
| Illite | 51 | 39 | 45 | 45 | 51 | 52 |
| $Ill_{70}Sm_{30}$ | 20 | 24 | 18 | 27 | 26 | 21 |
| $Ill_{90}Sm_{10}$ | 22 | 31 | 34 | 23 | 18 | 24 |

Cb: Clay beds; Sb: Silty beds.
Uc: upstream cake; Dc: Downstream cake.
MO: organic matter (550 °C); LOI: Lost Oxygen Index.
$Ill_pSm_q$: interstratified clays containing p% of illite sheets and q% of smectite sheets.

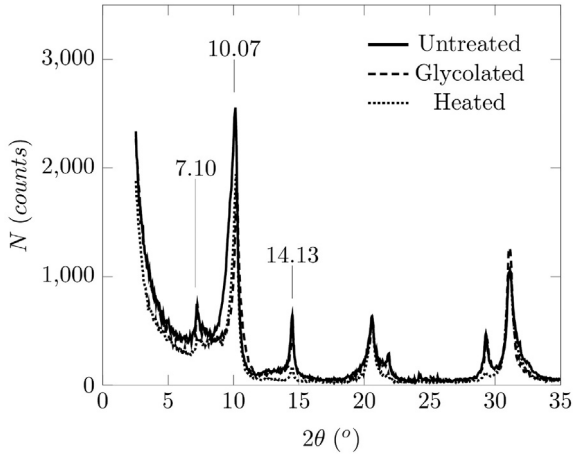


**Fig. 19.** Typical XRD diffractogram for silty beds of varved clays. The values above the peaks represent the basal distance between the clay layers (in Angstrom).

internal clogging on the nonwoven needle-punched geotextile, as indicated above (damaging of the brittle calcite crust during geotextile sampling, partial leaching of particles and embedded calcite compounds during hydraulic tests without confining soil). Moreover, the field permittivity is two orders of magnitude lower that the values calculated from our analytical model of internal clogging. Thus the performance of the trenches is probably not governed by the internal clogging mechanism.

### 4.3. Downstream chemical clogging

Chemical analyses (Table 6) showed that calcite accounts for 90% of the crust material on the downstream side of the nonwoven needle-punched geotextile (trench T3). This result is consistent with the observations of previous studies on granular filters which reported that more than 50% of the clogging material was calcium

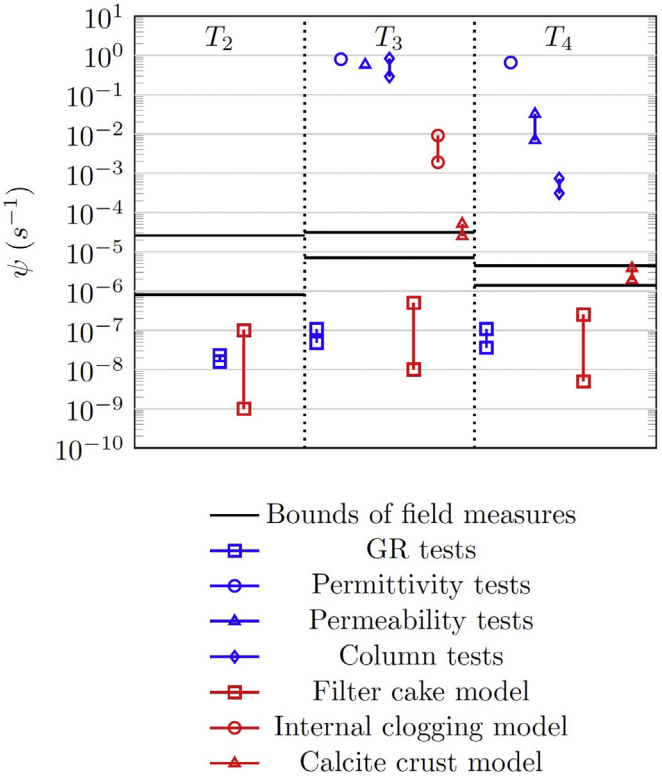


**Fig. 20.** Synthesis of the permittivity estimates for the field measures, laboratory tests and analytical models.

carbonate (Brune et al., 1994; Fleming et al., 1999). The behavior of calcium carbonate in a near-surface environment is primarily determined by the need for equilibrium in the reaction given by Equation (8):

$$Ca^{2+} + 2HCO_3^- \rightleftarrows CaCO_3 + H_2O + CO_2. \quad (8)$$

Equation (8) shows that calcite precipitation is controlled by the carbon-dioxide ($CO_2$) concentration. If the initial system is at equilibrium, then the calcite dissolves if the $CO_2$ concentration increases; conversely, the calcite precipitates if the $CO_2$ concentration decreases. When water passes through the aerobic medium of the trench, where the $CO_2$ concentration is very low, the $CO_2$ evaporates from the water, causing its concentration in the water to decrease abruptly, which in turn causes the calcite to precipitate. A higher $CO_2$ gradient leads to more calcite precipitation. Thus, by decreasing the $CO_2$ gradient through the geotextile, the microstructure and thickness of the geotextile influences the calcite precipitation rate within and downstream of the geotextile. In nonwoven needle-punched gotextiles, the calcite may thus precipitate over a larger geotextile thickness and over a larger fiber surface. This may explain why calcite precipitation is more pronounced in terms of thickness downstream of the woven-strip geotextile than downstream of the nonwoven needle-punched geotextile.

On the downstream side of the woven-strip geotextile (trench T4), clogging was localized around the pores of the geotextile where the strips intersect. The calcite precipitate was present both upstream and downstream of the geotextile. The siliceous material represented less than 3% of the crust (Table 6), which suggests that the clay particles were not retained by the geotextile before clogging and could no longer pass through the geotextile after clogging. The good performance of the geotextile measured in the laboratory may be explained by the cracks that are visible within the calcite

crust (Fig. 18(b)). These cracks may have formed when handling the geotextile during the dismantling and sampling processes. They may explain the disparities on the hydraulic permittivities observed in the field and in the laboratory.

The porous microstructure of the downstream calcite crust should have allowed water drainage and limited the filtration of clay particles. In particular, the channels were probably responsible for the hydraulic properties of the calcite crust. Assuming a mean channel diameter equal to 50 $\mu$m and a laminar flow regime, the flow rate passing through one of these channels $q$ can be estimated by Poiseuille's law given by Equation (9):

$$q = \frac{\rho_w}{\eta_w} \frac{\pi d_c^4}{128\, t} \Delta h \tag{9}$$

where $d_c$ is the representative diameter of the channels (m) and $t$ the thickness of the crust (m). Let us denote $N$ the number of channels per unit area ($m^{-2}$) and $\alpha$ the efficiency coefficient which corresponds to the ratio between the efficient drainage surface and the total surface of the geotextile. The permittivity of the calcite crust can be expressed as follows:

$$\psi = \alpha\, N \frac{\rho_w}{\eta_w} \frac{\pi d^4}{128\, t} \Delta h \tag{10}$$

The surface density of channels $N$ can be estimated from the stereo-microscopic views within the range $3–4 \cdot 10^5$ $m^{-2}$ for the nonwoven needle-punched geotextile (T3) and around $1–2 \cdot 10^5$ $m^{-2}$ for the woven strip geotextile (T4). The type of microstructure seems to influence the density of the channels. However, due to the damage of the calcite crust during the dismantling work, it was difficult to perform a reliable quantitative evaluation of this parameter.

The in plane permeability of the nonwoven needle-punched geotextile enabled us to use the whole remaining surface to drain the incoming flow. The efficient drainage surface corresponds to the surface of the geotextile deduced from the surface in direct contact with the pebbles. Thus, the efficiency coefficient can be roughly estimated as $\alpha = 0.5$. For the woven strip geotextile, only the surface in contact with the channels developed within the upstream cake concurred with the drainage of the incoming flow. Based on the observations made during the dismantling works, if we consider that the network of these channels, which were certainly not situated behind the pebbles, represents 10% of the surface of the geotextile, we obtain $\alpha = 0.10$. Considering the range of crust thickness values (Table 2), we obtain permittivity values ranging from $5.1 \cdot 10^{-5}$ $s^{-1}$ for trench T3 to $3.8 \cdot 10^{-6}$ $s^{-1}$ for trench T4 (Fig. 20). These values are in the range of the field values and the results suggest that the calcite crust formation is likely to be the main mechanism causing the decrease in trench performance.

## 5. Conclusions

Throughout their 18 years of service under specific hydraulic and physicochemical conditions, both types of geotextile filters (nonwoven needle-punched and woven strip geotextiles) used in the trenches were subjected to three phenomena that could potentially alter their filtration performance: *i)* the formation of filter cake upstream of the geotextile, *ii)* clogging of geotextile pores by fine particles and calcite compounds, and *iii)* the formation of a calcite crust on the downstream face of the geotextile. Based on in situ and laboratory analyses of the 18-year-old soil/geotextiles/pebbles interfaces composing the geotextile filters, the following conclusions were drawn:

- Over their 18 years of service, the geotextiles performed well in terms of mechanical resistance and filtration properties;
- The loss of hydraulic performance of the trenches can be attributed to the geotextile filters,
- Quantification of the overall performance of the entire geotextile filter is complicated by the fragility of the calcite crust. In particular, the results obtained for the woven-strip geotextile filter remain tentative,
- The geotextile interfaces were subjected to binding by a granular filter cake, to internal clogging, and to downstream chemical clogging by calcite precipitation, and
- The primary mechanism underlying the decrease in the hydraulic performance of the geotextile filters was found to be the formation of a calcite crust on the downstream face of the geotextiles (trenches T3 and T4) or drained soil (control trench T2).

These conclusions must be placed in perspective regarding the complexity and heterogeneity of the field conditions, where the relative weight of each clogging mechanism in the overall performance of the trenches and their interaction may vary from one part of the geotextile to another. Further works are required to develop models to simulate the chemical clogging mechanism and to calibrate them on the basis of laboratory experiments.

## Acknowledgments

The authors thank the Commissariat du Massif des Alpes (DATAR/FNADT/CIMA), the Conseil Général de l'Isère (CG38), the Société Nationale des Chemins de Fer (SNCF), the Pôle Grenoblois d'Etudes et de Recherches pour la Prévention des Risques Naturels (PGERPRN), and the Institut pour la Recherche appliquée et l'Expérimentation en génie civil (IREX) for funding this research program. The authors also thank the owners and tenants of the experimental site, the PELISSARD company, the operatives of the Office National des Forêts (ONF), and Laboratoire d'étude des Transferts en Hydrologie et Environnement (LTHE). We thank Matthieu Barthe, Roland Gallo and Alain Thomas, Alain Bernard, Faustine Byron, Yves Grémeaux and Sylvie Nicaise, Pierre Philippe, Nadia Benahmed (Irstea) and Jean-François Serratrice (Cerema) for their help during the dismantling work, the laboratory tests and the interpretation of the results.

## References

AFNOR, 1983. NF G 38016-textiles articles à usages industriels, essais des géotextiles, mesure de la permittivité hydraulique.
AFNOR, 1989. NF G 38017-textiles articles à usages industriels, essais des géotextiles, porométrie: détermination de l'ouverture de filtration.
AFNOR, 1996. NF P94-056-sols: reconnaissance et essais – analyse granulométrique – méthode par tamisage à sec après lavage.
AFNOR, 1999. NF EN ISO 13934-1-Textiles – Tensile Properties of Fabrics – Part 1: Determination of Maximum Force and Elongation at Maximum Force Using the Strip Method.
AFNOR, 2005. NF EN ISO 9862-Geosynthetics – Sampling and Preparation of Test Specimens.
AFNOR, 2008. NF EN ISO 10319-Geosynthetics Wide-width Tensile Test.
AFNOR, 2010. NF EN ISO 11058-Geotextiles and Geotextiles-Related Products. Determination of Water Permeability Characteristics Normal to the Plan, without Load.
AFNOR, 2010. NF EN ISO 12956-Geotextiles and Geotextile-related Products. Determination of the Characteristic Opening Size.
ASTM, 1996. D5101-Standard Test Method for Measuring the Soil-geotextile Clogging Potential by the Gradient Ratio.
Bhatia, S., Mlynarek, J., Rollin, A., Lafleur, J., 1991. Effect of pores structure of nonwoven geotextiles on their clogging behavior. In: Proceedings of the Geosynthetics 1991 Conference, vol. 2, pp. 629–642.
Brune, M., Ramke, H., Collins, H., Hanert, H., 1994. Incrustation problems in land-fill drainage systems. In: Christenson, T.H., Cossu, R., Stegmann, R. (Eds.), Landfilling of Waste: Barriers. E&FN Spon, London, U.K, pp. 569–605.
Carrier, W., Beckman, J., 1984. Correlations between index tests and the properties of remoulded clays. Géotechnique 34 (2), 211–228.

Cassidy, P., Mores, M., Kerwick, D., Koeck, D., 1990. Recent advances in the chemical compatibility evaluation of geosynthetic materials. In: Hoedt, D. (Ed.), 4th International Conference on Geotextiles, Geomembranes and Related Products. Balkema, pp. 685–688.
Christopher, B., Fischer, G., 1992. Geotextile filtration principles, practices and problems. Geotext. Geomembr. 11, 337–353.
Cooke, A., Rowe, R., 2008. 2d modelling of clogging in landfill leachate collection systems. Can. Geotech. J. 45 (10), 1393–1409.
Cooke, A., Rowe, R., Rittmann, B., Fleming, I., 1999. Modelling biochemically driven mineral precipitation in anaerobic biofilms. Water Sci. Technol. 39 (7), 57–64.
Dean, W.J., 1974. Determination of carbonate and organic matter in calcareous sediments and sedimentary rocks by loss on ignition: comparison with other methods. J. Sediment. Petrol. 44 (1), 242–248.
Degoutte, G., 1987. Practical examples of geotextile used in small earth dams. Geotext. Geomembr. 5, 239–250.
Duvall, D., 1995. Environmental degradation of pet and its potential effect on long-term mechanical properties of oriented pet products. Polym. Plast. Technol. Eng. 34 (2), 227–242.
Fannin, R., Vaid, Y., Shi, Y., 1994. Filtration behaviour of nonwoven geotextiles. Can. Geotech. J. 31 (4), 555–563.
Faure, Y., Baudoin, A., Pierson, P., Plé, O., 2006. A contribution for predicting geotextile clogging during filtration of suspended solids. Geotext. Geomembr. 24, 11–20.
Faure, Y., Farkouh, B., Delmas, P., Nancey, A., 1999. Analysis of geotextile filter behaviour after 21 years in valcros dam. Geotext. Geomembr. 17, 353–370.
Faure, Y.H., Fry, J.J., 2004. Rétention et colmatage des géotextiles. In: 5ème Rencontres Géosynthtiques Francophones 2003/2004 Colmar-Lille-Avignon, France, pp. 41–66.
Fleming, I., Barone, F., Dewaele, P., 2010. Case study – clogging of a geotextile/geopipe system in a landfill drainage application. In: 9th International Conference on Geosynthetics, pp. 1127–1130.
Fleming, I., Rowe, R., 2004. Laboratory studies of clogging of landfill leachate collection and drainage systems. Can. Geotech. J. 41 (1), 134–153.
Fleming, I., Rowe, R., Cullimore, D., 1999. Field observations of clogging in a landfill leachate collection system. Can. Geotech. J. 36, 685–707.
Germanique, J., 1994. Major, trace and rare earth elements in fourteen GSJ reference samples. determination by x-ray fluorescence spectrometry and inductively coupled plasma absorption emission spectrometry. Geostand. Newsl. 18 (1), 91–100.
Giraud, A., Antoine, P., van Asch, T.J.W., Nieuwenhuis, J.D., 1991. Geotechnical problems caused by glaciolacustrine clays in the French Alps. Eng. Geol. 31, 185–195.
Giroud, J., 1982. Filter criteria for geotextiles. In: Second International Conference on Geotextiles, vol. 1, pp. 103–108.
Giroud, J., 1996. Granular filters and geotextile filters. In: Geo-filters', vol. 96, pp. 565–680.
Giroud, J., Bonaparte, R., Beech, J., Gross, B., 1990. Design of soil layer geosynthetic systems overlying voids. Geotext. Geomembr. 9 (1), 11–50.
Gourc, J., Faure, Y., 1990. Soil particle, water, and fiber-a fruitful interaction now controlled. In: 4th International Conference on Geotextiles, Geomembranes and Related Products, pp. 949–971.
Halse, Y., Koerner, R., Lord Jr., A., 1987. Effect of high levels of alkalinity on geotextiles. part 1:$Ca(OH)_2$ solutions. Geotext. Geomembr. 5, 261–282.
Heerten, G., 1993. Filters in Geotechnical and Hydraulic Engineering. Ch. A contribution to the improvement of dimensioning analogies for grain filters and geotextile filters. Balkema, Rotterdam, pp. 121–127.
Hsuan, Y., Shroeder, H., Rowe, K., Mller, W., Greenwood, J., Cazzuffi, D., Koerner, R., 2008. Long-term performance and lifetime prediction of geosynthetics. In: EuroGeo4, pp. 1–40.
Junqueira, F., Silva, A., Palmeira, E., 2006. Performance of drainage systems incorporating geosynthetics and their effect in leachate properties. Geotext. Geomembr. 24 (5), 311–324.
Koerner, G., Koerner, R., 1992. Leachate flow rate behavior through geotextile and soil filters and possible remediation methods. Geotext. Geomembr. 11, 401–430.
Koerner, G., Koerner, R., 1995. Leachate Clogging Assessment of Geotextile and Soil Landfill Filters (Tech. rep.). U.S. Environmental Protection Agency.
Koerner, R., 1994. Designing with Geosynthetics. Prentice-Hall, New Jersey, Englewood Cliffs, N.J.
Koerner, R., Lord Jr., A., Halse, Y., 1988. Long-term durability and aging of geotextiles. Geotext. Geomembr. 7 (1–2), 147–158.
Kossendey, T., 1999. Long-term performance assessed from compatibility tests. Geotext. Geomembr. 17, 281–298.
Lafleur, J., 1999. Selection of geotextiles to filter broadly graded cohesionless soils. Geotext. Geomembr. 17 (5), 299–312.
Lafleur, J., Mlynarek, J., Rollin, A., 1992. Filter criteria for well graded cohesionless soils. In: First International Conference Geo-filters', vol. 92, pp. 97–106.
Leflaive, E., 1988. Durability of geotextiles: the french experience. Geotext. Geomembr. 7, 23–31.
Ling, H., Tatsuoka, F., 1993. Hydraulic conductivity of geotextiles under typical operational conditions. Geotext. Geomembr. 12, 509–542.
Luettich, S.M., Giroud, J.P., Bachus, R.C., 1992. Geotextile filter design guide. Geotext. Geomembr. 11 (4–6), 355–370.
Mannsbart, G., Christopher, B., 1997. Long-term performance of nonwoven geotextile filters in five coastal and bank protection projects. Geotext. Geomembr. 15, 207–221.
Mathur, A., Netravali, A., O'Rourke, T., 1994. Chemical aging effects on the physico-mechanical properties of polyesther and polypropylene geotextiles. Geotext. Geomembr. 13, 591–626.
McIsaac, R., Rowe, R., 2006. Effect of filter-separators on the clogging of leachate collection systems. Can. Geotech. J. 43, 674–693.
Mendonca, M., Ehrlich, M., 2006. Column test studies of ochre biofilm formation in geotextile filters. J. Geotech. Geoenviron. Eng. 132 (10), 1284–1292.
Miche, H., Simler, R., Affaton, P., Mickala, O., Boudzoumou, F., Mbina, M., 2013. New computerized method for the geochemical classification of precambrian carbonate rocks: case of a set of african cap carbonates. Int. J. Geosci. 4, 37–49.
Mlynarek, J., 1998. Designing geotextile filters part 1: soil filtration. In: 51st Canadian Geotechnical Conference, pp. 499–505.
Moore, D., Reynolds, R., 1989. X-ray Diffraction and the Identification and Analysis of Clay Minerals. Oxford, New York.
Murray, R.W., Miller, D.J., Kryc, K.A., 2000. Analysis of Major and Trace Elements in Rocks, Sediments, and Interstitial Waters by Inductively Coupled Plasma-atomic Emission Spectrometry (icp-aes). ODP Technical Note 29, pp. 1–27.
Narejo, D.B., 2003. Opening size recommendations for separation geotextiles used in pavements. Geotext. Geomembr. 21 (4), 257–264.
Nieuwenhuis, J., Van Genuchten, P., 1986. Feasability of highway crossing through landslide area on varved clays. In: 5th IAEG Congress. Balkema, Rotterdam, pp. 1705–1712.
Palmeira, E., Beirigo, E.A., Gardoni, M., 2010. Tailings-nonwoven geotextile filter compatibility in mining applications. Geotext. Geomembr. 28 (2), 136–148.
Palmeira, E., Gardoni, M., 2000. The influence of partial clogging and pressure on the behaviour of geotextiles in drainage systems. In: Geosynthetics International 7(4–6) (Special Issue on Liquid Collection Systems), pp. 403–431.
Palmeira, E.M., Gardoni, M.G., 2002. Drainage and filtration properties of nonwoven geotextiles under confinement using different experimental techniques. Geotext. Geomembr. 20 (2), 97–115.
Palmeira, E.M., Matheus, E., 2000. Gradient ratio tests on artificially clogged nonwoven geotextiles. In: Wolski, W., Mlynarek, J. (Eds.), Filters and Drainage in Geotechnical and Environmental Engineering, Proceedings of the 3rd International Conference Geofilter'2000, pp. 149–156.
Palmeira, E.M., Remigio, A., Ramos, M., Bernardes, R., 2008. A study on biological clogging of nonwoven geotextiles under leachate flow. Geotext. Geomembr. 26, 205–219.
Palmeira, E.M., Tatto, J., Araujo, G., 2012. Sagging and filtration behaviour of nonwoven geotextiles overlying different bedding materials. Geotext. Geomembr. 31, 1–14.
Rollin, A., Lombard, G., 1988. Mechanisms affecting long-term filtration behaviour of geotextiles. Geotext. Geomembr. 7, 119–145.
Rowe, R., 2005. Long-term performance of contaminant barrier systems. Gotechnique 55 (9), 631–678.
Rowe, R., Yu, Y., 2010. Factors affecting the clogging of leachate collection systems in MSW landfills. In: Proceedings of 6th International Congress on Environmental Geotechnics, New Delhi, India, November 2010, pp. 3–23.
Sounga, J., Miche, H., Noack, Y., Affaton, P., Mialoundama, F., 2012. Comparaison des rsultats analytiques obtenus aprs fusion alcaline au mtaborate avec ceux obtenus aprs fusion alcaline au ttraborate dans les niveaux d'altration des grs de l'inkisi (secteur de brazzaville, rpublique du congo): applications dans l'tude des profils d'altration. Afr. Geosci. Rev. 19 (3), 151–168.
Testemale, J.-P., Faure, Y.-H., Parron, C., Lambert, S., Royet, P., Fagon, Y., 1999. Filtre géotextile du barrage de torcy le vieux (saone et loire): prélèvements, analyses et interprétations. Ing. E A T 1, 31–39.
van der Sluys, L., Dierickx, W., 1987. The applicability of Darcy's law in determining the water permeability of geotextiles. Geotext. Geomembr. 5, 283–299.
van Genuchten, P.M.B., 1989. On the temporal and spacial variance displacement velocity of a slide in varved clays in the French Alps. Earth Surf. Process. Landf. 14, 565–576.
van Genuchten, P.M.B., van Asch, T.J.W., 1988. Factors controlling the movement of a landslide in varved clays near la mure (french alps). Bull. Société Géol. 8, 461–469.
Van Schoors, L., Lavaud, S., Duragrin, D., Barberis, N., 2009. Durability of polyester geotextiles in moderately alcaline medium. In: Rencontres Géosynthétiques 2009. French Committee on Geosynthetics, pp. 201–207.
Veylon, G., Barthe, M., Mriaux, P., Bernard, A., Gallo, R., Faure, Y.-H., 2012. Ageing of geotextiles in drainage systems – field observations. In: 5th European Geosynthetics Congress, Valencia, Spain, September 2012. Balkema.
Wu, C., Hong, Y., Yan, Y., Chang, B., 2006. Soil-nonwoven geotextile filtration behavior under contact with drainage materials. Geotext. Geomembr. 24, 1–10.
Yu, Y., Rowe, R., 2012. Modelling leachate-induced clogging of porous media. Can. Geotech. J. 49, 877–890.